Thermal and chemical evolution in the early Solar System as recorded by FUN CAIs: Part II – Laboratory evaporation of potential CMS-1 precursor material

Ruslan A. Mendybaev[1,2*], Curtis D. Williams[3§], Michael J. Spicuzza[4], Frank M. Richter[1,2], John W. Valley[4], Alexei V. Fedkin[1,2] and Meenakshi Wadhwa[3].

[1]Department of the Geophysical Sciences, [2]Chicago Center for Cosmochemistry, University of Chicago, Chicago, IL 60637, United States

[3]School of Earth and Space Exploration, Arizona State University, Tempe, AZ 85287, United States

[4]Department of Geoscience, University of Wisconsin, Madison, WI 53706, United States

*Corresponding author – Ruslan A. Mendybaev (ramendyb@uchicago.edu)

[§]Present address: Department of Earth and Planetary Sciences, University of California-Davis, Davis, CA 95616, United States

Submitted to Geochimica et Cosmochimica Acta

March 28th, 2016

Revised on July 25th, 2016

ABSTRACT

We present the results of laboratory experiments in which a forsterite-rich melt estimated to be a potential precursor of Allende CMS-1 FUN CAI was evaporated into vacuum for different lengths of time at 1900ºC. The evaporation of this melt resulted in residues that define trajectories in chemical and magnesium, silicon and oxygen isotopic composition space that come very close to the measured properties of CMS-1. The isotopic composition of the evaporation residues was also used to determine the kinetic isotopic fractionation factors [$\alpha_{2,1}$ (vapor-melt) defined as the ratio of isotopes 2 and 1 of a given element in the evaporating gas divided by their ratio in the evaporating source] for evaporation of magnesium ($\alpha_{25,24}$ for $^{25}Mg/^{24}Mg$), silicon ($\alpha_{29,28}$ for $^{29}Si/^{28}Si$) and oxygen ($\alpha_{18,16}$ for $^{18}O/^{16}O$) from the forsterite-rich melt at 1900ºC. The values of $\alpha_{25,24}$ = 0.98383±0.00033 and $\alpha_{29,28}$ = 0.99010±0.00038 are essentially independent of change in the melt composition as evaporation proceeds contrary to $\alpha_{18,16}$ which changes from $\alpha_{18,16}$ = 0.9815±0.0016 to $\alpha_{18,16}$ ~ 0.9911 when the residual melt composition changes from forsteritic to melilitic. Using the determined values of $\alpha_{25,24}$ and $\alpha_{29,28}$ and present-day bulk chemical composition of the CMS-1, composition of the precursor of the inclusion was estimated to be close to the clinopyroxene+spinel+forsterite assembly condensed from a solar composition gas. The correspondence between the chemical composition and isotopic fractionation of experimental evaporation residues and the present-day bulk chemical and isotopic compositions of CMS-1 is evidence that evaporation played a major role in the chemical evolution of CMS-1.

1. INTRODUCTION

Calcium-, aluminum-rich inclusions (CAIs) are the oldest known materials to have formed in the Solar System (e.g., Amelin et al., 2002, 2010; Bouvier and Wadhwa, 2010; Connelly et al., 2012). The most extensively studied CAIs are coarse-grained Type B inclusions composed mainly of melilite, spinel, fassaite and anorthite, and Compact Type A (CTA) inclusions composed mainly of melilite (>60 vol%), spinel, perovskite and often Ti-rich fassaite (e.g., Grossman, 1975, 1980; Simon et al., 1999; MacPherson, 2007). All Type B CAIs and majority of CTAs are believed have been formed by crystallization of partially molten droplets, and the coarse-grained texture of the Type B CAIs has been reproduced in laboratory dynamic crystallization experiments (e.g., Stolper and Paque, 1986; Beckett et al., 1990; Mendybaev et al., 2006) when partially molten droplets were cooled from ~1450ºC at less than 50ºC per hour. Typical Type B and CTA CAIs are characterized by well resolved mass-dependent fractionations of magnesium, silicon and oxygen isotopes (e.g., δ^{25}Mg up to 11‰ relative to Burma spinel and δ^{29}Si up to 5‰ relative to NBS-28 quartz; see Grossman et al., 2000; 2008 and references therein) which are attributed to a Rayleigh-type distillation. The correlated mass-dependent fractionations of silicon and magnesium isotopes have been also found in laboratory experiments in which CAI-like melts were evaporated in low-pressure conditions (Richter et al., 2002, 2007; Knight et al., 2009; Mendybaev et al., 2013a).

Most FUN CAIs (CAIs with Fractionation and Unidentified Nuclear effects, Wasserburg et al., 1977) are similar to isotopically "normal" (non-FUN) CAIs in terms of their bulk chemical and mineral compositions (see Clayton et al., 1984; Davis et al., 1991; Krot et al., 2014; Williams et al., 2016 and references therein). However, in contrast to normal CAIs, the classical FUN CAIs display little or no excess of radiogenic ^{26}Mg, and are characterized by

large mass-dependent isotopic fractionation of magnesium and silicon (δ^{25}Mg up to ~40‰ and δ^{29}Si up to ~15‰), distinct oxygen isotopic composition of their high-temperature minerals, and mass-independent isotopic anomalies of unknown origin in a number of elements. Some of these CAIs are characterized by large kinetic mass-dependent isotope fractionation effects and lack mass-independent anomalies ("F" or FUN-like CAIs, such as TE; e.g., Clayton et al. 1984), while other CAIs have large nuclear anomalies without significant kinetic isotope fractionation ("UN" CAIs, e.g., Ireland, 1988). Mass-dependent fractionation of magnesium, silicon and oxygen isotopes observed in CAIs are usually associated with their evaporation under low-pressure conditions that results in faster evaporation of lighter isotopes and thus enrichments of the evaporation residues in heavy isotopes (e.g., Esat et al., 1986; Davis et al., 1990; Ireland et al., 1992; Wang et al., 2001; Richter 2002, 2007; Yamada et al., 2006; Knight et al., 2009). Recent experiments by Mendybaev et al. (2010, 2013a,b) showed that evaporation of a MgO- and SiO_2-rich melt in vacuum results in the evaporation residues with chemical and isotopic compositions of magnesium, silicon and oxygen close to the levels measured in FUN (and FUN-like) CAIs.

On a three-oxygen isotope diagram (Fig. 1) the oxygen isotopic compositions of FUN and FUN-like CAIs is distinctly different from that of "normal" CAIs and plot to the right of the CCAM (Carbonaceous Chondrite Anhydrous Mineral) mixing line with slope ~1 defined by minerals in the "normal" CAIs (Clayton et al., 1977). The isotopic composition of spinel, forsterite and often pyroxene in the FUN CAIs fall along a mass-fractionation line (FUN FL) with slope ~1/2 that is parallel to the mass-dependent terrestrial fractionation line (TFL) but significantly displaced with typical Δ^{17}O ~-24‰, although some FUNs, such as TE, are less ^{16}O-rich with Δ^{17}O up to -16.4‰ (e.g., Krot et al., 2014). The oxygen isotopic compositions of

mineral grains along FUN FL are believed to reflect the crystallization sequence of minerals from an evaporating melt. The degree of mass-dependent oxygen isotopic fractionation due to evaporation, as estimated from the difference between the $\delta^{18}O$ (or $\delta^{17}O$) of the most fractionated grains along FUN FL and the initial $\delta^{18}O$ (or $\delta^{17}O$) values at the intersection of the FUN FL and CCAM lines (see Fig. 1), can be as high as 40-45‰ in $\delta^{18}O$ or 20-22‰ in $\delta^{17}O$ (see for examples, Clayton et al., 1977, 1984; Davis et al., 1991, 2000; Krot et al., 2014; Williams et al., 2016). Such high degrees of mass-dependent oxygen isotope fractionation were also observed in the evaporation experiments (Davis et al., 1990; Wang et al., 2001; Mendybaev et al., 2013a) along with enrichment in heavy magnesium and silicon isotopes. The correlated mass-fractionated effects in Mg, Si and O isotopes in both vacuum experiments and FUN and FUN-like CAIs clearly indicate that these CAIs have experienced high degrees of melting in the solar nebula, which resulted in evaporation of very significant amounts of the moderately volatile elements.

CMS-1 is a FUN CAI that was recently identified in the Allende CV3 chondrite and is described in detail in the accompanying paper (Williams et al., 2016). It is a coarse-grained CAI of irregular shape (approximately 3 x 5 mm in overall maximum dimensions) and contains several rounded cavities filled with matrix material. CMS-1 has an igneous texture and is composed of 39% melilite, 30% Ti-Al-rich pyroxene, 24% spinel with minor amounts of hibonite and perovskite along its margins. Chemically it consist of 34.8 wt% Al_2O_3, 25.4 wt% SiO_2, 23.9 wt% CaO, 11.9 wt% MgO, 1.4 wt% FeO, 1.1 wt% TiO_2 and small amounts of Na_2O, K_2O, Cr_2O_3 and Cl_2O (Williams et al., 2016). CMS-1 is highly enriched in heavy magnesium and silicon isotopes [a weighed means of $\delta^{25}Mg$ and $\delta^{29}Si$ are 32.72±0.50‰ and 15.54±0.27‰ (95% confidence interval) respectively; Williams et al., 2016], and shows a large range of

~32‰ in $\delta^{18}O$ (~16‰ in $\delta^{17}O$) values caused by the evaporation (Fig. 1). To explain such large mass-fractionation effects in magnesium, silicon and oxygen isotopes by evaporation we report the results of a new set of laboratory evaporation experiments in which a melt with an estimated CMS-1 precursor composition was evaporated to varying degrees in a high vacuum furnace. The resulting set of evaporation residues will be referred to as the FUNC residues. Their bulk chemical composition as well as their magnesium, silicon and oxygen isotopic compositions were measured and compared to those of CMS-1.

2. SOME THEORETICAL ASPECTS OF VACUUM EVAPORATION

It was shown (e.g., Richter et al., 2002; 2007) that laboratory evaporation of silicate melts in vacuum can be successfully described by the standard Hertz-Knudsen formulation (see Hirth and Pound, 1963):

$$J_i = \sum_{j=1}^{n} \frac{n_{ij}\gamma_{ij}P_{ij}}{\sqrt{2\pi m_{ij}RT}} \quad (1)$$

where J_i is the net evaporative flux (in moles per unit area per time) of a component i (element or isotope), n_{ij} is the number of atoms of i in the jth gas species containing i, γ_{ij} is the evaporation coefficient for the jth gas species containing i, P_{ij} is the saturation vapor pressure of j, m_{ij} is the molar mass of the gas species j that would be in equilibrium with the melt, R is the gas constant, and T is the absolute temperature. In case of magnesium and silicon evaporating from silicate melts, the equilibrium gas is predominantly $Mg_{(g)}$ and $SiO_{(g)}$ as was determined experimentally (e.g., Nichols et al., 1995), and Eq. (1) can be simplified as:

$$J_{Mg} = \frac{\gamma_{Mg}P_{Mg}}{\sqrt{2\pi m_{Mg}RT}} \quad (2)$$

and

$$J_{SiO} = \frac{\gamma_{SiO} P_{SiO}}{\sqrt{2\pi m_{SiO} RT}}, \quad (3)$$

where J_{Mg} and J_{SiO}, are the evaporative fluxes of magnesium and silicon, γ_{Mg} and γ_{SiO} are the empirical evaporation coefficients of $Mg_{(g)}$ and $SiO_{(g)}$, P_{Mg} and P_{SiO} are their vapor pressures in equilibrium with the condensed phase, m_{Mg} and m_{SiO} are their masses, and T is the absolute temperature. The relative evaporation rates of magnesium and silicon can be calculated using relationship:

$$\frac{J_{Si}}{J_{Mg}} = \frac{\gamma_{SiO} P_{SiO}}{\gamma_{Mg} P_{Mg}} \sqrt{\frac{m_{Mg}}{m_{SiO}}} \quad (4)$$

if the evaporation coefficients and equilibrium vapor pressures are known. The evaporation coefficients need to be determined experimentally as they cannot be calculated theoretically, and it was found that the values of γ_{Mg} and γ_{SiO} determined from vacuum evaporation experiments using silicate melts (e.g., Richter et al., 2007; Knight et al., 2009) are quite different from unity although the reason of such deviations remains unknown. Equilibrium speciation and vapor pressures of the evaporating gases can be measured experimentally using Knudsen cells technique (e.g., Nichols et al., 1995), but we do not measure them in our experiments and use thermodynamic calculations to estimate the relevant vapor pressures.

Eq. (1) also describes the kinetic fractionation of isotopes in vacuum. Similarly to Eq. (4), the ratio of the fluxes of isotopes *1* and *2* of a given element *i* can be expressed as:

$$\frac{J_{i,2}}{J_{i,1}} = \frac{\gamma_{i,2} P_{i,2}}{\gamma_{i,1} P_{i,1}} \sqrt{\frac{m_{i,1}}{m_{i,2}}} = R_{2,1} \frac{\gamma_{i,2}}{\gamma_{i,1}} \sqrt{\frac{m_{i,1}}{m_{i,2}}} \quad (5)$$

again assuming that the element *i* evaporates predominantly as a single gas species; $R_{2,1}$ is the atomic ratio of isotopes *2* and *1* in the evaporating source. The ratio of the isotopic fluxes $J_{i,2}/J_{i,1}$ in the evaporating gas to the atomic ratio $R_{2,1}$ defines the isotopic fractionation factor $\alpha_{2,1}$

($a_{2,1} = \gamma_{i,2}/\gamma_{i,1}\sqrt{m_{i,1}/m_{i,2}}$). When the fractionation factor $\alpha_{2,1}$ is unchanging as evaporation proceeds the isotopic composition of the evaporation residues evolve via Rayleigh fractionation (e.g., Esat, 1984; Davis et al., 1990, 2015; Richter et al., 2002, 2004, 2007) given as:

$$R_{2,1} = R_0 f_i^{\alpha_{2,1}-1} \quad (6)$$

or

$$\ln(R_{2,1}/R_0) = (\alpha_{2,1} - 1)\ln f_i \quad (7)$$

where $R_{2,1}$ is the ratio of isotopes *2* and *1* of a given chemical element *i* in the evaporation residue, R_0 is their isotopic ratio in the starting material prior to evaporation, f_i is the fraction of the isotope *1* remaining in the residue after evaporation.

The Rayleigh fractionation relationships given above will be used here to calculate the chemical and isotopic fractionations during vacuum evaporation of the FUNC forsteritic melt.

3. EXPERIMENTAL TECHNIQUE

3.1 Starting materials and experimental procedure

The starting material containing 37.9 wt% MgO, 11.6 wt% Al_2O_3, 42.9 wt% SiO_2 and 7.6 wt% CaO was evaporated in vacuum (<10^{-9} bars) at 1900ºC. The composition, chosen as a potential precursor of CMS-1, was obtained by adding MgO and SiO_2 to the reported bulk composition of the inclusion (Williams et al., 2016) in such amounts that when sufficiently evaporated this material would be expected to produce fractionations in Mg and Si isotopes close to δ^{25}Mg = 32.72±0.50‰ and δ^{29}Si = 15.54±0.27‰ reported by Williams et al. (2016) for CMS-1. Here we assumed that evaporation of the CMS-1 precursor (FUNC melt) would fractionate magnesium and silicon isotopes the same way (i.e., the isotopic fractionation factors will remain the same) as was determined from evaporation experiments with forsteritic FUN1

and FUN2 melts (Mendybaev et al., 2013a) with significantly different bulk chemical compositions than the FUNC melt. The mixture of MgO (Alfa Aesar, 99.998%), SiO_2 (Aldrich®, >99.995%), Al_2O_3 (Alfa Aesar®, 99.99%), and $CaCO_3$ (Alfa Aesar®, 99.99%) was homogenized in the Retsch® MM200 oscillating mill using a 5 ml agate jar and two 7 mm agate balls under ethanol at 20.0 cycles per second for at least 400 min. After the mixture was dried at room temperature, it was placed into a platinum crucible that was heated to 1000°C for ~10 h to drive off CO_2 from the calcium carbonate. The mixture of oxides then was cooled and stored for later use in a desiccator connected to a vacuum pump. Individual evaporation experiments were conducted on samples with 25–40 mg of the mixture loaded onto 2.5 mm diameter iridium wire loops.

The vacuum evaporation experiments were run in a high-temperature high-vacuum furnace at the University of Chicago (see Hashimoto, 1990 for the furnace details). After the sample was placed into the furnace at room temperature, it was pumped down to about 10^{-7} bars, and the temperature was then raised to 1400ºC at 20ºC/min and held at this temperature for about 20 min to allow the sample to degas. Once the furnace pressure had dropped to ~10^{-9} bars, the temperature was raised to 1900ºC at 40ºC/min and the sample allowed to evaporate for a predetermined amount of time (from 0 to 55 minutes). An experiment was ended by cutting the power to the heating elements (see Mendybaev et al., 2013a for the details). The evaporation residue was removed from a cold furnace and broken into several pieces for separate chemical and isotopic analysis. The experiment (FUNC-5 in Tables 1 and 2) in which the sample was quenched immediately after the furnace temperature reached 1900°C (i.e., run duration at 1900°C is zero minutes) is referred as a “zero-time” run.

3.2 Analytical techniques

3.2.1 Chemical composition of evaporation residues.

The texture and chemical composition of the FUNC evaporation residues were studied using a JEOL JSM-5800LV scanning electron microscope equipped with an Oxford/Link ISIS-300 energy-dispersive X-ray (EDX) microanalysis system at the University of Chicago. The working conditions involved a 15 keV accelerating voltage and a 0.4 nA beam current with natural and synthetic materials used as calibration standards. The chemical composition of the samples was determined either by averaging at least 20 spots analyzed across the sample (for the residues that quenched to glass) or by averaging the results of scanning 15-20 areas of ~250×200 microns in dimension for the residues that quenched to intergrowth of forsterite and glass.

3.2.2 Magnesium and silicon isotopic analyses.

Isotopic composition of magnesium and silicon of the FUNC evaporation residues was measured using a Photon Machine Analyte 193 laser ablation system connected to a ThermoFinnigan Neptune MC-ICPMS (multicollector inductively coupled plasma mass spectrometer) at the Arizona State University (see accompanying paper by Williams et al. for details). Magnesium isotopes (^{24}Mg, ^{25}Mg and ^{26}Mg as well as ^{27}Al) were measured simultaneously during one session; silicon isotopes (^{28}Si, ^{29}Si and ^{30}Si) were also measured simultaneously but in a separate analytical session. All isotopic measurements were conducted in high-resolution mode using 100 to 275 μm diameter spot sizes depending on the magnesium and silicon concentrations of the sample. The measurements consisted of approximately 320 s of data acquisition per spot with forty 8 s integrations. Individual samples were bracketed by a

synthetic B133R-10 glass with a bulk composition similar to that of a typical Type B CAI (Richter et al., 2007; Janney et al., 2011). The magnesium isotopic composition of B133R-10 relative to DSM3 is δ^{25}Mg=-1.77±0.16‰ and δ^{26}Mg=-3.51±0.28‰ and that of silicon relative to NBS-28 is δ^{29}Si=0.00±0.15‰ and δ^{30}Si =-0.01±0.11‰. The details of the analytical procedure including the matrix effect corrections are given in Janney et al. (2011).

3.2.3 Oxygen isotopic analyses.

Oxygen isotopic composition of the FUNC samples was measured at the University of Wisconsin-Madison by laser fluorination of 1.5 to 2.9 mg chips. Oxygen produced by laser heating in a BrF_5 atmosphere was carefully purified by passing the released gas through a number of traps, converted to CO_2 on hot graphite, and analyzed for ^{16}O and ^{18}O with a Finnigan MAT 251 mass spectrometer. All measurements were made in one session. During the measurements, the δ^{18}O values of unknowns were adjusted down by 0.22‰ based on the average of six analyses of the UWG-2 garnet standard (δ^{18}O=5.80‰ VSMOW) that bracket unknown analyzes during the same session. The details of the analytical method and data standardization were described by Valley et al. (1995) and by Spicuzza et al. (2007). The correlation between δ^{18}O and δ^{17}O values in FUN1 and FUN2 evaporation residues (δ^{17}O =0.515 × δ^{18}O) reported previously by Mendybaev et al. (2010, 2013a) was used to calculate δ^{17}O values for the FUNC residues.

4. RESULTS

The textures of the quenched samples are very similar to those of the FUN1 and FUN2 evaporation residues (Fig. 3 of Mendybaev et al., 2013a). The least evaporated samples FUNC-

5 and FUNC-10 (Table 1) are composed of very fine grained intergrowths of forsterite and glass; the more evaporated samples (FUNC-1, -9, and -3) have a barred olivine texture similar to those in chondrules; and the most evaporated sample FUNC-6 appears as a clear homogeneous glass. The fact that the experimental temperature was above the melting temperature of forsterite (1890°C) and that forsterite was observed even in "zero-time" run residues (i.e., when the sample was quenched immediately after the furnace temperature reached 1900°C) indicates that forsterite is a product of the relatively slow quenching (~1000˚C/min) of the molten Mg_2SiO_4-rich droplets rather than crystallization during the high-temperature phase of the experiments.

4.1 Chemical composition of evaporation residues

Despite their textural differences we found that all evaporation residues are chemically homogeneous without any concentration gradients across the samples. The chemical composition of the starting FUNC material and evaporation residues is given in Table 1. Run durations listed in the Table are times during which samples were evaporated at 1900ºC. About 5% weight loss occurred even in the zero-time experiment as also indicated by lower SiO_2/Al_2O_3 and MgO/Al_2O_3 ratios in the FUNC-5 compared to the FUNC starting material. To compensate for the chemical and isotopic fractionations during the ramping up of the furnace temperature to 1900°C, we used the zero-time run residue as the effective starting composition. Table 2 shows the degree of the evaporation expressed as fractions of magnesium ($f_{^{24}Mg}$), silicon ($f_{^{28}Si}$) and oxygen ($f_{^{16}O}$) remaining in the evaporated residues and also the associated isotopic fractionations relative to that of the zero-time run. Because aluminum is very refractory and does not evaporate during the experiments, the values of $f_{^{24}Mg}$ were calculated as

$(MgO/Al_2O_3)_{residue}/(MgO/Al_2O_3)_{zero\text{-}time\ run}$ with corrections for contribution of ^{25}Mg and ^{26}Mg. (1.1% for the most evaporated sample FUNC-6). The $f_{^{28}Si}$ and $f_{^{16}O}$ were calculated in the same way.

Figure 2 shows the evaporation trajectory from the FUNC experiments in the anorthite – gehlenite – forsterite ternary diagram. The figure shows that as evaporation proceeds the composition of the evaporation residues (shown as filled circles) evolves from the forsterite stability field to the melilite stability field. Because CaO and Al_2O_3 do not evaporate from the melt at the conditions of the experiments, the plot of weight percents of SiO_2 versus MgO can be used to fully characterize the evaporation trajectory. The trajectory in SiO_2-MgO space is shown in Figure 3. Figures 2 and 3 also show evaporation trajectories of the FUN1 (open circles) and FUN2 (open diamonds) melts from Mendybaev et al. (2013a) evaporated at the same conditions and the bulk composition of CMS-1 CAI (FUNC shown as a star) normalized to 100% of $CaO+MgO+Al_2O_3+SiO_2$ (24.95 wt% CaO, 12.42 wt% MgO, 36.22 wt% Al_2O_3, 26.41 wt% SiO_2). The thin curve fitting the experimental residues in Fig. 3 is an evaporation trajectory of the FUNC melt calculated the same way as described by Grossman et al. (2000) with the ratio of evaporation coefficients of Mg (γ_{Mg}) and SiO (γ_{SiO}) used in Eq. (4) is equal to 2.1 (see section 4.1 for details). The composition of the gas phase in equilibrium with the melt along the calculated trajectory is shown in Figure 4 which illustrates that the major magnesium and silicon bearing species above the FUC melt are $Mg_{(g)}$ and $SiO_{(g)}$ as was also determined experimentally (e.g., Nichols et al., 1995) . Figures 2 and 3 illustrate that: 1) the evaporation of the silica-rich FUNC melt starts with faster evaporation of silicon compared to magnesium very much like what was observed in experiments of Richter et al. (2002, 2007) evaporating Type B CAI-like melt in vacuum, and opposite to what was observed in our experiments using the

magnesia-rich FUN1 melt in which magnesium initially evaporated faster than silicon; 2) after this initial evaporation step that lasted for ~15 min at 1900ºC, the evaporation trajectory of the FUNC melt converges with that of the FUN1 and FUN2 melts; 3) the evaporation trajectory of the FUNC melt passes very close to the composition of CMS-1 and it takes less than an hour to produce residues (FUNC-4 and FUNC-6, see Table 1) with chemical and isotopic compositions close to CMS-1; 4) the experimental evaporation trajectory of the FUNC melt can be nicely fit by a trajectory calculated using $\gamma_{Mg}/\gamma_{SiO} = 2.1$. This ratio is different from $\gamma_{Mg}/\gamma_{SiO} = 0.74$ used by Richter et al. (2007) to fit experimental data on the evaporation of a Type B CAI-like melt at 1600ºC and $\gamma_{Mg}/\gamma_{SiO} = 1.0$ to fit experimental data at 1800ºC and 1900ºC. The difference in γ_{Mg}/γ_{SiO} of melt trajectories in the melilite stability field reported by Richter et al. (2007) and those of melts in the forsterite stability field reported here are a clear indication that γ_{Mg}/γ_{SiO} depends not only on temperature but also on the composition of the starting materials evaporated. The change in the value of γ_{Mg}/γ_{SiO} from 2.1 to 1.0 as melt composition changes from forsteritic to melilitic explains the departure of the most evaporated experimental residue in Figs. 2 and 3 from the evaporation trajectory calculated using $\gamma_{Mg}/\gamma_{SiO} = 2.1$.

4.2 Magnesium, silicon and oxygen isotopic compositions of the FUNC evaporation residues

The magnesium, silicon and oxygen isotopic compositions of the FUNC evaporation residues expressed in the delta notation defined as

$$\delta^{X}Mg = 1000 \times \left[\frac{(^{X}Mg/^{24}Mg)_{sample}}{(^{X}Mg/^{24}Mg)_{standard}} - 1 \right] \quad \text{and} \quad \delta^{X}Si = 1000 \times \left[\frac{(^{X}Si/^{28}Si)_{sample}}{(^{X}Si/^{28}Si)_{standard}} - 1 \right],$$

for magnesium and silicon, for example, are listed in Table 1 relative to the starting materials. We found that isotopically all FUNC residues are uniform without any spatial variations in their Mg and Si isotopic compositions. As was noted above, to compensate for the isotopic fractionations during the ramping up the furnace temperature to 1900°C, the isotopic compositions of the run products were normalized to the zero-time residue (sample FUNC-5; $\delta^{29}Si\equiv0$, $\delta^{25}Mg\equiv0$, $\delta^{18}O\equiv0$) and listed in Table 2 as $\delta^{25}Mg_{t=0}$, $\delta^{26}Mg_{t=0}$, $\delta^{29}Si_{t=0}$, $\delta^{30}Si_{t=0}$, $\delta^{17}O_{t=0}$ and $\delta^{18}O_{t=0}$. Relationships between $\delta^{29}Si_{t=0}$ and $\delta^{25}Mg_{t=0}$, and $\delta^{18}O_{t=0}$ and $\delta^{25}Mg_{t=0}$ in the FUNC residues (all in permil) are shown in Figure 5 along with the measured average silicon and magnesium isotopic compositions of CMS-1 ($\delta^{25}Mg$ = 32.72±0.50‰, $\delta^{29}Si$ = 15.54±0.27‰; Williams et al., 2016) shown as the star. Oxygen isotopic composition of CMS-1 shown in Fig. 5 is our estimate of isotopic fractionation due to evaporation ($\Delta^{18}O$ ~32‰) obtained by the extent of the change in $\delta^{18}O$ along that portion of the isotopic fractionations that fall along the slope 1/2 line defined by the spinel grains (see Fig. 1 for details). Figure 5 shows that the isotopic composition of CMS-1 plots on or very close to the dashed curves which are the best fits through the FUNC experimental residues, and is within few permil of the fractionation in the most evaporated FUNC-6 residue ($\delta^{25}Mg_{t=0}$ = 35.0±0.3‰, $\delta^{29}Si_{t=0}$ = 16.6±0.1‰, and $\delta^{18}O_{t=0}$ = 29.1±0.1‰). The initially faster enrichments in heavy ^{29}Si relative to ^{25}Mg reflect the initially faster evaporation of silicon relative to magnesium seen in Figs. 2 and 3. Because under low vacuum conditions the SiO is expected to be the major evaporating gas containing oxygen (Fig. 4), one would also expect the initial faster enrichment of ^{18}O over ^{25}Mg, which is also seen in Fig. 5. The fact that the $\delta^{29}Si$, $\delta^{25}Mg$ and $\delta^{18}O$ of CMS-1 are very close to the isotopic trajectories in $\delta^{29}Si$- $\delta^{25}Mg$ and $\delta^{18}O$-$\delta^{25}Mg$ space of the FUNC evaporation residues is strong evidence that isotopic composition of CMS-1 reflects the effect of evaporation in the same way as in our laboratory experiments.

4.3 Kinetic isotope fractionation factor for silicon, magnesium, and oxygen

When a silicate melt evaporates in vacuum, mass-dependent isotopic fractionation takes place due to a faster evaporation of lighter isotopes of a given element relative to heavy ones. As a measure of the isotope fractionation we will use the kinetic isotopic fractionation factor $\alpha_{2,1}$ defined as the ratio of isotopes *2* and *1* of element *i* in the evaporating gas divided by their ratio in the evaporating source melt (see Eqs. (6) and (7) in section 2). It has often been assumed that the value of $\alpha_{2,1}$ is equal to the inverse square root of the ratio of masses of evaporating isotopes, which in the case of ^{25}Mg and ^{24}Mg, for example, would result in $\alpha_{25,24} = \sqrt{24/25} =$ 0.97980. It has been shown, however, that the experimentally measured values of $\alpha_{2,1}$, at least in the case of vacuum evaporation of silicon, magnesium and oxygen from silicate melts (e.g., Davis et al., 1990; Wang et al., 2001; Richter et al., 2002, 2007, Knight et al., 2009, Mendybaev et al., 2013), are significantly different from the theoretically expected values. In this section we use our experimental data on magnesium, silicon and oxygen isotopic fractionation during evaporation of FUNC forsterite-rich melt to determine the kinetic fractionations factors and compare them with those from our previous experiments.

Our estimate of the chemical composition of the starting FUNC melt that when sufficiently evaporated would result in a residue that is close chemically and isotopically to the CMS-1 FUN CAI, was made using Eq. (6) with values for the kinetic isotopic fractionation factors of $\alpha_{25,24}$ = 0.98372±0.00041 and $\alpha_{29,28}$ = 0.9899±0.0004 (Mendybaev et al., 2013a) between ^{25}Mg and ^{24}Mg and between ^{29}Si and ^{28}Si, respectively, during evaporation of FUN1 and FUN2 melts in vacuum at 1900ºC. The assumption that $\alpha_{25,24}$ and $\alpha_{29,28}$ for the FUNC melt would be close to those for the FUN1 and FUN2 forsteritic residues was based on our finding that despite significant difference in the starting bulk chemical compositions of FUN1 and FUN2 the values of $\alpha_{25,24}$ and $\alpha_{29,28}$ were the same. We can now test this assumption using the

results of the FUNC evaporation experiments listed in Table 2 to determine the values of $\alpha_{25,24}$ and $\alpha_{29,28}$, and also $\alpha_{18/16}$ for $^{18}O/^{16}O$.

As mentioned above we can use the elemental and isotopic composition of the sample from the zero-time experiment as the effective initial composition in equation (6). For $^{25}Mg/^{24}Mg$ the fractionation, equation (7) can be rewritten as

$$\ln(R/R_0) = (\alpha_{25,24} - 1)\ln f_{^{24}Mg} \quad (8)$$

where R=$^{25}Mg/^{24}Mg$ of the evaporation residue, R_o=$^{25}Mg/^{24}Mg$ in the zero-time run sample FUNC-5, $\alpha_{25,24}$ is the kinetic fractionation factor for $^{25}Mg/^{24}Mg$, and $f_{^{24}Mg}$ is the fraction of the ^{24}Mg in FUNC-5 remaining in the residue. According to equation (8) if the kinetic isotope fractionation due to evaporation is a Rayleigh process, then $ln(R/R_0)$ of a set of evaporation residues should be a linear function of $ln(f_{^{24}Mg})$ with a slope corresponding to $\alpha_{25,24} - 1$. This not only provides a way to accurately determine the value of $\alpha_{25,24}$ that fits the entire data set, but also serves to test and validate the key assumption that the process is indeed Rayleigh fractionation (e.g., Davis et al., 2015). The same approach outlined above was used to determine the isotopic fractionation factors $\alpha_{29,28}$ for the fractionation of ^{29}Si relative to ^{28}Si and $\alpha_{18,16}$ for the fractionation of ^{18}O relative to ^{16}O.

Figure 6 shows the magnesium isotopic composition of the FUNC evaporation residues given in Table 2 expressed as $1000*ln(R/R_0)$ versus fraction of ^{24}Mg remaining in the residue expressed as $-ln(f_{^{24}Mg})$. The magnesium isotopic data of the residues, when plotted in this way, fall along a line with slope $\alpha_{25,24} - 1$ corresponding to $\alpha_{25,24}$= 0.98383±0.00033, which within error is the same as $\alpha_{25,24}$= 0.98372±0.00041 for the FUN1 and FUN2 forsterite-rich residues (Mendybaev et al., 2013a) and 0.98417±0.00039 determined by Davis et al. (1990) for molten

Mg_2SiO_4, but different from $\alpha_{25,24}$ = 0.98607±0.00016 determined for Type B CAI-like melt (Richter et al., 2007). Most importantly, the experimentally obtained values of $\alpha_{25,24}$ are distinctly different from $\alpha_{25,24} = \sqrt{24/25} = 0.97980$.

Figure 7 is the same as Fig. 6 but for silicon isotopes. Similar to the magnesium data, the silicon isotopic compositions plot along a line with slope corresponding to $\alpha_{29,28}$ = 0.99010±0.00038 which is effectively the same as $\alpha_{29,28}$ = 0.9899±0.0004 determined for FUN1 and FUN2 evaporated in vacuum at 1900ºC (Mendybaev et al., 2013a) and $\alpha_{29,28}$ = 0.98985±0.00044 with no resolvable variations with temperature for Type B CAI-like melt (Knight et al., 2009). The experimentally obtained values of $\alpha_{29,28}$ are close to, but resolvable different, from $\alpha_{29,28} = \sqrt{m_{^{28}Si^{16}O} / m_{^{29}Si^{16}O}} \approx \sqrt{44/45} = 0.98883$.

Figure 8 shows that when the measured oxygen isotopic composition data for the FUNC residues are plotted in the same way as was done for the magnesium and silicon data, they fall along two distinct trends. The evaporation residues with bulk composition in forsterite stability field define a line with the slope corresponding to $\alpha_{18,16}$ = 0.9815±0.0016 which is effectively the same as for evaporation residues from molten Mg_2SiO_4 ($\alpha_{18,16}$ = 0.9805±0.0003; Davis et al., 1990), a solar composition melt ($\alpha_{18,16}$ = 0.9797±0.0030 at 2000ºC and 0.9795±0.00010 at 1800ºC calculated from the data of Wang et al., 2001), and the FUN1 and FUN2 residues ($\alpha_{18,16}$ = 0.9786±0.0015, Mendybaev et al., 2010, 2013a). The two most evaporated FUNC residues with bulk composition in the melilite field plot along a line with the slope corresponding to $\alpha_{18,16}$ ~ 0.9911, which is close to $\alpha_{18,16}$ ~ 0.9916 for the most evaporated FUN2 residues with composition in the melilite field (Mendybaev et al., 2010; 2013a).

5. DISCUSSION

A major goal of this study was to test by laboratory experiments if vacuum evaporation of an appropriately chosen the MgO- and SiO_2-rich melt could result in a residue with the chemical and isotopic compositions close to those of the natural CMS-1 FUN CAI, and if so, whether such a potential precursor of CMS-1 could be a condensate from a solar composition gas.

5.1 Chemical and isotopic composition of FUNC evaporation residues and CMS-1 FUN CAI

Two major processes that operate during evaporation of a melt in vacuum are: 1) evaporation from the melt/gas interface, and 2) supply of material from the inner parts of the molten droplet to the melt/gas interface by diffusion. The facts that all FUNC evaporation residues, including those quenched into forsterite+glass, are chemically and isotopically homogeneous (within the uncertainties) suggest that cation diffusion in the molten FUNC droplets at 1900ºC is fast compared to evaporation of Mg and Si from the surface of the melt and thus cannot be the rate-limiting step. Below we will discuss the results on evaporation of magnesium and silicon from the surface of FUNC melt.

5.1.1. Chemical composition

The evaporation of magnesium and silicon from silicate melts is expected to be dominated by the reactions:

$$MgO_{(melt)} \rightarrow Mg_{(g)} + 0.5O_{2(g)} \quad (9)$$

$$SiO_{2(melt)} \rightarrow SiO_{(g)} + 0.5O_{2(g)}. \quad (10)$$

Eqs. (2) and (3) indicate that the evaporation rates of magnesium and silicon, J_{Mg} and J_{SiO}, are proportional to the vapor pressure of their dominating gas species P_{Mg} and P_{SiO} in equilibrium

with the condensed phase (Fig. 4) and to the empirical evaporation coefficient γ_{Mg} and γ_{SiO}. If γ_{SiO} / γ_{Mg} ratio in Eq. (4) remains constant during evaporation, then the relative evaporation rates of silicon and magnesium at fixed temperature are controlled by the equilibrium P_{SiO} and P_{Mg} above the condensed phase, which for reactions (9) and (10) can be expressed as:

$$P_{Mg} = \frac{a_{MgO} \times K_{eq(9)}}{\sqrt{f_{O2}}} \quad \text{and} \quad P_{SiO} = \frac{a_{SiO2} \times K_{eq(10)}}{\sqrt{f_{O2}}},$$

where a_{MgO} and a_{SiO2} are the activities of MgO and SiO_2 in the melt (not to be confused with the isotopic fractionation factors of magnesium, silicon and oxygen expressed in this paper as $\alpha_{25,24}$, $\alpha_{29,28}$ and $\alpha_{18,16}$), and $K_{eq(9)}$ and $K_{eq(10)}$) are the equilibrium constants for reactions (9) and (10), respectively. The equation (4) thus transforms into:

$$\frac{J_{Si}}{J_{Mg}} \propto \frac{a_{SiO2}}{a_{MgO}}, \qquad (11)$$

with the constant of proportionality being the ratio of the equilibrium constants $K_{eq(9)}$ and $K_{eq(10)}$, which suggests that relative evaporation rates of silicon and magnesium are, to first order, proportional to the activities of MgO and SiO_2 in the melt. Thus in SiO_2-rich melts ($a_{SiO2} > a_{MgO}$) silicon will initially evaporate faster than magnesium, which will decrease a_{SiO2} (and increases a_{MgO}) until the a_{SiO2}/a_{MgO} ratio in the residual melt will reach some value at which the relative evaporation rates of silicon and magnesium, J_{Mg} / J_{SiO}, become constant. In MgO-rich melts ($a_{MgO} > a_{SiO2}$), on the other hand, magnesium will initially evaporate faster than silicon, which will decrease a_{MgO} (and increase a_{SiO2}) in the residual melt. As a result, during evaporation of any SiO_2- and MgO-rich melt the ratio a_{SiO2} / a_{MgO} is expected to settle around some value which will remain constant as evaporation proceeds. Figure 9 illustrates this behavior during evaporation of the FUNC melt at 1900ºC; the activities of SiO_2 and MgO in an evolving melt were calculated the same way as used by Grossman et al. (2008) but with γ_{SiO} /

γ_{Mg} = 2.1 which was the value used in Fig. 3 to fit the composition of the experimental FUNC residues. Comparing Figs. 3 and 9 one can see that the observed evaporation trajectory from vacuum experiments follows the thermodynamically expected pattern: evaporation starts with faster loss of SiO_2 relative to MgO, followed by essentially a linear trend with slope close to ~0.5 on the SiO_2 – MgO diagram (Fig. 3). The linear part of the trend in Fig. 3 converges with those of FUN1 and FUN2. The same convergence was observed in all our experiments when MgO- and/or SiO_2-rich forsteritic melts were evaporated at the same conditions (Mendybaev et al., 2014). As the FUNC melt continues to evaporate, the composition of the residual melts becomes melilitic as illustrated in Fig. 2, and thus spinel, melilite and pyroxene observed in CMS-1 are expected to crystallize from this evolved melt as it cools.

5.1.2. Isotopic composition

The faster initial evaporation of SiO_2 over MgO from the FUNC melt in vacuum discussed above causes an initially higher degree of fractionation of silicon and oxygen isotopes (silicon evaporates mostly as $SiO_{(g)}$, see Fig.4) compared to magnesium as reflected in the shape of $\delta^{29}Si_{t=0}$ and $\delta^{18}O_{t=0}$ *vs.* $\delta^{25}Mg_{t=0}$ curves in Figure 5. We should note, however, that the initially faster losses of silicon and oxygen compared to magnesium from the FUNC melt does affect their isotopic fractionation factors: Figs. 6, 7 and 8 show that all experimental residues with composition within the forsterite stability field plot along a single line with $\alpha_{25,24}$= 0.98383±0.00033, $\alpha_{29,28}$ = 0.99010±0.00038 and $\alpha_{18,16}$ = 0.9815±0.0016. This, along with the fact that the experimentally obtained value of $\alpha_{25,24}$, $\alpha_{29,28}$ and $\alpha_{18,16}$ for FUNC are within error the same as for forsteritic FUN1, FUN2 and Mg_2SiO_4 melts, suggests that the kinetic isotopic fractionation factor is independent of chemical composition of melts in the forsterite field. On

the other hand, the above value of $\alpha_{25,24}$ is significantly different from $\alpha_{25,24}$ = 0.98607±0.00016 determined by Richter et al. (2007) for the melilitic Type B CAI-like melt and $\alpha_{25,24}$ = 0.98567±0.00046 obtained by Mendybaev et al. (2013a) for the most evaporated (i.e., melilitic) FUN2 experimental residues. The similar changes in the isotopic fractionation factor were also observed for oxygen isotopes: from $\alpha_{18,16}$ = 0.9815±0.0016 for melts in the forsterite field to $\alpha_{18,16}$ ~ 0.9911 for the FUNC residues in the melilite field and from $\alpha_{18,16}$ = 0.9786±0.0015 to $\alpha_{18,16}$ ~ 0.9916 for the FUN2 residue compositions within the forsterite field and melilite field, respectively. The fractionation factors for silicon isotopes were found to be the same both for forsteritic and melilitic melts: $\alpha_{25,24}$ = 0.99010±0.00038 within the whole range of compositions for the FUNC melt (Fig. 7) which is the same as $\alpha_{29,28}$ = 0.9899±0.0004 determined for FUN1 and FUN2 melt (Mendybaev et al., 2013a) and $\alpha_{29,28}$ = 0.98985±0.00044 for the melilitic Type B CAI-like melt (Knight et al., 2009). The reason why the isotopic fractionation factors depend on melt composition for some elements but not for others remains unclear. It might be result of changes in the melt structure as it evolves from forsteritic (SiO_4^{2-} network structure) to melilitic ($S_2iO_7^{6-}$ network structure) with associated polymerization of SiO_4 ^{2}monomers into S_2iO_7 $^{6-}$ dimmers resulting in release of free oxygen (see Mysen et al., 1982 and references therein). The fact that there are no abrupt changes in the equilibrium speciation of the gas phase above the evaporating melt (Fig. 4) eliminates the gas phase being responsible for the changes in the isotopic fractionation factors.

As it was also noted earlier, the experimentally determined values of the isotopic fractionation factors shown in Figs. 6, 7 and 8 are distinctly different from values calculated as the inverse square root of the ratio of mass of the isotopes. Lack of resolvable dependence of $\alpha_{25,24}$ on sample size found in experiments when the melilitic Type B CAI-like droplets 1–6 mm

in size were evaporated in vacuum (Richter et al., 2007) and in low-pressure H_2 furnace (Parsad et a., 2000) along with theoretical arguments, allowed Richter et al. (20007) to make a persuasive case that the reason for the observed departure of the experimental fractionation factors from the inverse square root value was not the result of recondensation in the experiments. The implication is that the departure is due to the evaporation coefficients themselves being mass-dependent (i.e. $\gamma_{i,1}/\gamma_{i,2} \neq 1$).

Figure 10 shows the oxygen isotopic composition in individual minerals of CMS-1 CAI and in the FUNC evaporation residues. Because only $\delta^{18}O$ of the FUNC residues was measured, the $\delta^{17}O$ values were calculated from the correlation between $\delta^{18}O$ and $\delta^{17}O$ measured previously in FUN1 and FUN2 evaporation residues ($\delta^{17}O = 0.515 \times \delta^{18}O$, Mendybaev et al., 2010, 2013a). We also assumed that the starting FUNC melt and precursor of CMS-1 had oxygen isotopic composition $\delta^{17}O$=-49‰ and $\delta^{18}O$ =-48‰ (the values at the intersection of CCAM and FUN fractionation lines). Figure 10 shows that not only the FUNC oxygen isotopic composition evolves along the same FUN FL as established by spinel grains of CMS-1, but it also covers the range of the oxygen isotopic compositions measured. This again strongly indicates that evaporation played a major role during formation and evolution of FUN (and FUN-like) CAIs and is responsible for their enrichments in heavy isotopes.

5.2 Chemical composition of the precursor of CMS-1.

The vacuum evaporation of the FUNC melt for 55 min at 1900ºC resulted in a residue (FUNC-6) with chemical and magnesium, silicon, and oxygen isotope compositions close to that of CMS-1. This suggests that our initial choice of the possible precursor of CMS-1 was

quite reasonable and thus its composition should be close to that of the zero-time FUNC-5 residue: 34.1 wt% MgO, 13.9 wt% Al_2O_3, 42.9 wt% SiO_2 and 9.1 wt% of CaO.

The precursor composition of CMS-1 can also be calculated using Eq. (6) to determine the amounts of MgO and SiO_2 evaporated given the isotopic composition of magnesium and silicon in CMS-1 and the experimentally determined values of $\alpha_{25,24}$ and $\alpha_{29,28}$ (Figs. 6 and 7). This amount of evaporated magnesium and silicon is then added back to the present-day bulk composition of the inclusion to give an estimate of its precursor. Using the values of δ^{25}Mg = 32.72±0.50‰ and δ^{29}Si = 15.54±0.27‰ for CMS-1 CAI (Williams et al., 2016) and fractionation factors $\alpha_{25,24}$ = 0.98383±0.00033 for ^{25}Mg/^{24}Mg and $\alpha_{29,28}$ = 0.99010±0.00038 for ^{29}Si/^{28}Si, the estimates of the fraction of original magnesium and silicon remaining in the inclusion calculated using relationship (6) and taking into account abundance ratios of magnesium (Catanzaro et al., 1966) and silicon (Coplen et al., 2002) isotopes would be $f_{^{24}Mg}$ ~ 0.128 to 0.148 and $f_{^{28}Si}$ ~ 0.193 to 0.229. These estimated values also take into account uncertainties both in the measured isotopic fractionations in CMS-1 CAI and in the experimentally determined fractionation factors $\alpha_{25,24}$ and $\alpha_{29,28}$. Thus the CMS-1 precursor composition can be estimated by adding back ~85 to 87% of lost magnesium and ~77 to 81% of lost silicon to the present-day bulk composition of the inclusion normalized to 100% of MgO+CaO+Al_2O_3+SiO_2 (24.95 wt% CaO, 12.42 wt% MgO, 36.22 wt% Al_2O_3, 26.41 wt% SiO_2) and renormalizing again to 100% and is shown in Fig. 11 as a cloud of open circles with composition ranging from ~29 to 36 wt% MgO and ~41.0 to 49 wt% SiO_2 (CaO/Al_2O_3=0.69). The range of the estimated CMS-1 precursor composition is somewhat SiO_2-rich compared to the equilibrium assembly of clinopyroxene+spinel+forsterite which in a solar composition gas is stable from ~1260K to 1290K at $P_{H2}=10^{-5}$ bars (from ~18 to 45 wt% MgO in Fig. 11) and from

~1370K to 1415K at $P_{H2}=10^{-3}$ bars (from ~26.5 to 46.5 wt% MgO in Fig. 11). It should be mentioned that increasing MgO content of the present-day composition of CMS-1 CAI by 3 wt% and lowering SiO_2 content by 3 wt% would shift the cloud of CMS-1 precursors to the right by 6.5 wt% along x-axis and down by 6 wt% along y-axis, and onto the calculated solar gas condensation curve. There are various reasons why the measured present-day bulk composition of CMS-1 FUN CAI might be uncertain by as much as several wt%. First, the reported bulk chemical composition of CMS-1 FUN CAI is based on analyses of one section which might not reflect the average bulk composition of the inclusion. Furthermore, the reported CaO/Al_2O_3 ratio of CMS-1 (0.69) is significantly lower than the solar ratio of 0.792, which could mean that the reported composition does not represent the inclusion as a whole, or that the precursor of CSM-1 was not a direct condensate from an exact solar composition gas but rather is an aggregate of early solar system condensates mixed in different proportions.

Regardless of whether CMS-1 precursor was or was not a direct condensate from a solar composition gas, its isotopic compositions clearly indicate that the precursor has experienced a relatively short but energetic thermal processing under low-pressure conditions in the solar nebula which caused its melting and evaporation of substantial amounts of magnesium, silicon, and oxygen. Given that the CMS-1 precursor was undoubtedly very forsterite-rich, a sufficient degree of melting at above the solidus of ~1300ºC (Osborn et al., 1969; our calculated liquidus temperature is 1532ºC which is close to that of Osborn and Gee, 1969) will be required to produce significant amount of melt to allow such massive volatilization and isotopic fractionation. In order to produce the observed enrichments in heavy magnesium and silicon isotopes of the order of $\delta^{25}Mg \sim 30 – 40‰$ and $\delta^{29}Si = 15 – 20‰$ by evaporation in a solar gas at $P_{H2}= 10^{-4}$ bar, it would take only a few minutes if precursor material had evaporated at

1900ºC and not much more than about an hour if evaporated at 1600°C (see Richter et al., 2002, 2007; Mendybaev et al., 2013b for the effect of P_{H2} and temperature on the evaporation rates of silicate melts). We should note that evaporation of magnesium and silicon from the CMS-1 precursor would lower the liquidus of the residual melt such that in a solar nebula environment the droplet will remain molten as it cools and will continue to evaporate at temperatures significantly less than 1600ºC.

5.3 Laboratory evaporation experiments and natural FUN CAIs.

Figures 3 and 5 illustrate that a simple isothermal evaporation in vacuum at 1900ºC of the FUNC starting material results in a residue trajectory that passes very close to Allende FUN CAI CMS-1 by simultaneously fitting its reported chemical and isotopic composition. To the best of our knowledge, the only FUN CAIs other than the one studied here for which the bulk chemical and silicon, magnesium and oxygen isotopic compositions have been reported are Allende C1 and Vigarano 1623-5 (see Mendybaev et al, 2013a). Despite this lack of reported bulk chemical composition for other FUN (and FUN-like) CAIs, we can still test whether the correlations between the various isotopic fractionations in these CAIs are comparable to those of the experimental evaporation residues. Figure 12 compares the relationships between δ^{29}Si versus δ^{25}Mg and δ^{18}O versus δ^{25}Mg in FUN (and FUN-like) CAIs for which the relevant data have been reported (Clayton et al., 1978; 1984, 1988; Brigham, 1990; Davis et al., 1991; Thrane et al., 2008; Williams et al., 2012, 2013, 2015) with that from the FUNC, FUN1, and FUN2 evaporation residues with composition in the forsterite stability field (Fig. 2 and residues with MgO > 15 wt% in Fig. 3). Figure 12a shows that most of the natural FUN CAIs plot close to a line with slope ~0.5 (shown as the solid red line) as was observed in the forsteritic FUN1 and

FUN2 residues. The magnesium and silicon isotopic composition of B7F6 plots well above the solid line, while those of EK-1-4-1, 1623-5 and BG82DH8I plot below it. The higher degree of fractionation of silicon isotopes relative to magnesium isotopes in B7F6 could be explained if its precursor was more highly enriched in SiO_2 relative to MgO, which would cause faster initial evaporation of silicon relative to magnesium and results in a higher initial enrichment in δ^{29}Si compared to δ^{25}Mg as was observed in the FUNC experiments (closed circles and dotted line in Fig. 12). On the other hand, if the precursor of a FUN CAI was originally more highly enriched in MgO relative to SiO_2, the faster evaporation of magnesium relative to silicon would result in the δ^{29}Si *vs.* δ^{25}Mg trajectory plotting below the solid line in Fig. 12.

The oxygen isotopic composition of the FUN residues (Fig. 12*b*) also correlates reasonably well with the magnesium isotopic composition. Considering that estimating the degree of oxygen isotopic fractionation due to evaporation is not entirely straightforward (oxygen isotopic compositions of some minerals in the FUN CAIs, like melilite or anorthite, were modified later in their history due to processes not related to evaporation, such as the isotopic exchange between the ^{16}O-rich molten droplet and ^{16}O-poor nebular gas after the evaporation stage ended), the correspondence between the δ^{18}O and δ^{25}Mg of the other FUN CAI minerals with the correlation line defined by the experimental evaporation residues is surprisingly good. The high degree of isotopic fractionation of silicon, magnesium and oxygen of CMS-1 and the other FUN CAIs is clear evidence that they experienced at least one very high-temperature heating event that caused melting and evaporation of significant amounts of their silicon, magnesium and oxygen and the associated fractionation of their isotopes. The degree of melting and evaporation experienced by the precursors of FUN CAIs was

significantly higher than that of "normal" Type B or CTA CAIs which are characterized by significantly smaller (few permil) isotopic fractionations of silicon, magnesium and oxygen.

6. CONCLUSIONS

The chemical and isotopic composition of experimental residues produced by evaporation of a silicon– and magnesium–rich melt at 1900ºC in vacuum together with the properties of CMS-1 FUN CAIs allow us to conclude:

1) Evaporation of the forsteritic FUNC melt in a simple one-stage heating process in vacuum at 1900ºC for less than an hour resulted in a residue with bulk chemical and isotopic compositions very close to that of Allende FUN CAI CMS-1. If the evaporation had taken place in a low-pressure hydrogen-dominated solar nebula gas, it would have taken only a few minutes at 1900ºC and less than an hour at 1700ºC to evaporate ~80% of silicon and ~85% of magnesium from a precursor material to produce enrichments in heavy silicon and magnesium isotopes to the levels comparable to what is measured in CMS-1 (δ^{29}Si =15.5±0.27‰ and δ^{25}Mg = 32.7±0.50‰). These very short timescales suggest that the precursor of CMS-1 experienced very energetic (>1700ºC) short duration event(s) that resulted in at least partial melting and significant evaporation of silicon, magnesium and oxygen.
2) The experimentally determined kinetic isotopic fractionation factors $\alpha_{25,24}$= 0.98383±0.00033, $\alpha_{29,28}$ = 0.99010±0.00038 and $\alpha_{18,16}$ = 0.9815±0.00016 for the forsterite-rich FUNC melt are within error the same as reported previously for FUN1 and FUN2 forsterite-rich melts. As residual melt enters the melilite stability field, $\alpha_{18,16}$

changes to ~0.9911 which is close to that of the most evaporated FUN2 melt reported by Mendybaev et al. (2013).

3) Using the present-day bulk chemical and isotopic compositions of CMS-1 of Williams et al. (2016) and the experimentally determined values for $\alpha_{25,24}$ and $\alpha_{29,28}$, we estimated that the CMS-1 precursor was a forsterite-rich object containing ~29 to 36 wt% MgO and ~41.0 to 49 wt% SiO_2 which is close to but somewhat more silica-rich than the clinopyroxene+spinel+forsterite assembly that is stable in a solar composition gas at 1370–1410K at $P_{H2}=10^{-3}$ bars and 1260–1290K at $P_{H2}=10^{-5}$ bars. These temperatures are significantly lower than that required to melt the CMS-1 precursor (solidus ~1300ºC, liquidus 1532ºC) to a very high degree such that evaporation of silicon and magnesium from such melt would result in the isotopic fractionations measured in the CMS-1 CAI.

Acknowledgements:

We thank T. Esat, A. El Goresy, T. Ireland (A.E.) and anonymous reviewer for their comments and suggestions which improved this paper. This work was supported by NASA grants MNX13AH09G S01 (to FMR) and NNX11AK56 (to MW), and by NSF grant EAR-1524336 (to JWV).

REFERENCES

Amelin Y., Krot A. N., Hutcheon I. D., and Ulyanov A. A. (2002) Lead isotopic ages of chondrules and calcium-aluminum-rich inclusions. *Science* **297**, 1678–1683.

Amelin Y., Kaltenbach A., Iizuka T., Stirling C. H., Ireland T. R., Petaev M., and Jacobsen S. B. (2010) U-Pb chronology of the Solar System's oldest solids with variable 238U/235U. *Earth Planet. Sci. Lett.* **300**, 343–350.

Beckett J. R., Spivack A. J., Hutcheon I. D., Wasserburg G. J., and Stolper E. M. (1990) Crystal chemical effects on partitioning of trace elements between mineral and melt: An experimental study of melilite with application to refractory inclusions from carbonaceous chondrites. *Geochim. Cosmochim. Acta* **54**, 1755−1774.

Bouvier A. and Wadhwa (2010) The age of the Solar System redefined by the oldest Pb-Pb age of a meteoritic inclusion. *Nature Geosci.* **3**, 637–641.

Catanzaro E. J., Murphy T. J., Garner E. L., and Shields W. R. (1966) Absolute isotopic abundance ratios and atomic weights of magnesium. *J. Res. Natl. Bur. Stand.* **70a**, 453–458.

Clayton R. N. (1993) Oxygen isotopes in meteorites. *Annu. Rev. Earth Planet. Sci*., **21**, 115–149.

Clayton R. N. and Mayeda T. K. (1977) Correlated O and Mg isotopic anomalies in Allende inclusions: I. Oxygen. *Geophys. Res. Lett*., **4**, 295–298.

Clayton R. N., Onuma N., Grossman L., and Mayeda T. K. (1977) Distribution of the pre-solar component in the Allende and other carbonaceous chondrites. *Earth Planet Sci. Lett*., **34**, 209-224.

Clayton R. N., MacPherson G. J., Hutcheon I. D., Davis A. M., Grossman L., Mayeda T. K., Molini-Velsko C., and Allen J. M. (1984). Two forsterite-bearing FUN inclusions in the Allende meteorite. . *Geochim. Cosmochim. Acta* **48**, 535−548.

Clayton R. N., Hinton R. W., and Davis A. M. (1988) Isotopic variations in the rock-forming elements in meteorites. *Phil. Trans. Roy. Soc. London*, **325**, 483–501.

Conard R. (1976) A study of the chemical composition of Ca-Al-rich inclusions from the Allende meteorite. MS. Thesis, Oregon State University.

Connelly J. N., Bizzarro M., Ivanova M., and Krot A. N. (2011) Towards a new absolute chronology for the early Solar System. *Formation of the First Solids in the Solar System*, LPI Contribution No. 1639, #9056.

Coplen T. B., Böhlke J. K., De Bièvre P., Ding T., Holden N. E., Hopple J. A., Krouse H. R., Lamberty A., Peiser H. S., Révész K., Rieder S. E., Rosman K. J. R., Roth E., Taylor P. D. P., Vocke R. D. Jr., and Xiao Y. K. (2002) Isotope-abundance variations of selected elements. *Pure. Appl. Chem.* **74**, 1987–2017.

Davis A. M., Hashimoto A., Clayton R. N., and Mayeda T. K. (1990) Isotope mass fractionation during evaporation of Mg_2SiO_4. *Nature* **347**, 655–658.

Davis A. M., MacPherson G. J., Clayton R. N., Mayeda T. K., Sylvester P. J., Grossman L., Hinton R. W., Laughlin J. R. (1991) Melt solidification and late-stage evaporation in the evolution of a FUN inclusion from the Vigarano C3V chondrite. *Geochim. Cosmochim. Acta* **55**, 621−637.

Davis A. M., McKeegan K. D., MacPherson G. J. (2000) Oxygen-isotopic compositions of individual minerals from the FUN Inclusion Vigarano 1623-5. *Meteoritics & Planetary Science* 35: Suppl., A47.

Davis A. M., Richter F. M., Mendybaev R. A., Janney P. E., Wadhwa M., and McKeegan K. D. (2015) Isotopic mass fractionation laws for magnesium and their effects on ^{26}Al–^{26}Mg systematics in solar system materials. *Geochim. Cosmochim. Acta* **39**, 2458–261.

Esat T. M. (1984) A 61 cm radius multi-detector mass spectrometer at the Australian National University. *Nucl. Instrum.Meth. Phys. Res.* **B5**, 545–553.

Esat T. M., Spear R. H., and Taylor S. R. (1986) Isotope anomalies induced in laboratory distillation. *Nature*, **319**, 576–578.

Georg, R. B., Reynolds, B. C., Frank, M. & Halliday, A. N. (2006) New sample preparation techniques for the determination of Si isotopic composition using MC-ICPMS. *Chem. Geol.* **235**, 95–104.

Grossman L. (1975) Petrology and mineral chemistry of Ca-rich inclusions in the Allende meteorite. *Geochim. Cosmochim. Acta* **39**, 438–451.

Grossman L. (1980) Refractory inclusions in the Allende meteorite. *Annu. Rev. Earth Planet. Sci.* **8**, 559–608.

Grossman L., Ebel D. S., Simon S. B., Davis A. M., Richter F. M., and Parsad N. M. (2000) Major element chemical and isotopic compositions of refractory inclusions in C3 chondrites: the separate roles of condensation and evaporation. *Geochim. Cosmochim. Acta* **64**, 2879–2894.

Grossman L., Simon S. B., Rai V. K., Thiemens M. H., Hutcheon I. D., Williams R. W., Galy A., Ding T., Fedkin A. V., Clayton R. N., Mayeda T. K. (2008) Primordial compositions of refractory inclusions. *Geochim. Cosmochim. Acta* **72**, 3001–3021.

Ireland T. R. (1988) Correlated morphological, chemical, and isotopic characteristics of hibonites from the Murchison carbonaceous chondrites. . *Geochim. Cosmochim. Acta* **52**, 2827−2839.

Ireland T. R., Zinner E. K., Fahey A. J., and Esat T. M. (1992) Evidence for distillation in the formation of HAL and related hibonite inclusions. *Geochim. Cosmochim. Acta* **56**, 2503−2520.

Janney P. E., Richter F. M., Davis A. M., Mendybaev R. A., and Wadhwa M. (2005) Silicon isotope ratio variations in CAI evaporation residues measured by laser ablation multicollector ICPMS. *Lunar Planet Sci.* **36**, #2123 (CD-ROM).

Janney P. E., Richter F. M., Mendybaev R. A., Wadhwa M., Georg R. B., Watson E. B., and Hines R. R. (2011) Matrix effects in the analysis of Mg and Si isotope ratios in natural and synthetic glasses by laser ablation-multicollector ICPMS: a comparison of single- and double-focusing mass spectrometers. *Chem. Geol.* **281**, 26–40.

Hashimoto A. (1990) Evaporation kinetics of forsterite and implications for the early solar nebula. *Nature*, **347**, 53–55.

Hirth J. P. and Pound G. M. (1963) *Condensation and Evaporation. Nucleation and Growth Kinetics*. Progress in Materials Science, Vol. XI, Macmillan, 191 pp.

Knight, K. B., Kita, N. T., Mendybaev, R. A., Richter, F. M., Davis, A. M. & Valley, J. W. (2009) Silicon isotope fractionation of CAI-like vacuum evaporation residues. *Geochim. Cosmochim. Acta* **73**, 6390–6401.

Krot A. N., Nagashima K., Hutcheon I.D., Davis A.M., Thrane K., Bizzarro M., Huss G. R., Papanastassiou D. A., and Wasserburg G. W. (2008) Oxygen isotopic compositions of

individual minerals from FUN CAIs. *XXXIX Lunar and Planetary Science Conference*, CD-ROM, Abstract #2162, Lunar and Planetary Institute (CD-ROM).

Krot A. N., Nagashima K., Ciesla F. J., Meyer B. S., Hutcheon I.D., Davis A.M., Huss G. R., and Scott E. R. D. (2010) Oxygen isotopic compositions of the sun and mean oxygen isotopic composition of the protosolar silicate dust: Evidence from refractory inclusions. *Astrophys. J.*, **713**, 1159–1166.

Krot A. N., Nagashima K., Wasserburg G. J., Huss G. R., Papanastassiou D., Davis A. M., Hutcheon I. D., and Bizzarro M. (2014) Calcium-aluminum-rich inclusion with fractionation and unknown nuclear effects (FUN CAIs): I. Mineralogy, petrology, and oxygen isotopic compositions. *Geochim. Cosmochim. Acta* **145**, 206–247.

Lugmair G. W. and Shukolyukov A. (2001) Early solar system events and timescales. *Meteorit. Planet. Sci.* **36**, 1017–1026.

MacPherson G. J. (2007) Calcium-aluminum-rich inclusions in chondritic meteorites. In *Meteorites, Planets, and Comets* (A. M. Davis, ed.), Vol. 1 *Treatise on Geochemistry* (H. D. Holland and K. K. Turekian, eds.), Electronic edition, Elsevier, Oxford, published electronically at http://www.sciencedirect.com/science/referenceworks/9780080437514.

MacPherson G. J., Paque J. M., Stolper E., and Grossman L. (1984) The origin and significance of reverse zoning in melilite from Allende Type B inclusions. *J. Geol.*, 92, 289–305.

Mendybaev R. A., Richter F. M., and Davis A. M. (2006) Crystallization of melilite from CMAS-liquids and the formation of the melilite mantle of Type B1 CAIs: Experimental simulations. *Geochim. Cosmochim. Acta* **70**, 2622 – 2642.

Mendybaev R. A., Richter F. M., Spicuzza M. J. and Davis A. M. (2010) Oxygen isotope fractionation during evaporation of Mg- and Si-rich CMAS liquids in vacuum. *Lunar Planet. Sci.* **41**, #2725.

Mendybaev R. A., Richter F. M., Georg R. B., Janney P. E., Spicuzza M. J., Davis A. M., and Valley J. W. (2013a) Experimental evaporation of Mg- and Si-rich melts: Implication for the origin and evolution of FUN CAIs. *Geochim. Cosmochim. Acta* **123**, 368 – 384.

Mendybaev R. A., Teng F.-Z., Georg R. B. and Richter F. M. (2013b) Magnesium and silicon isotopic fractionations during evaporation of forsterite-rich melts: The temperature and composition effects. *Lunar Planet. Sci.* **44**, #3017.

Mendybaev R. A., Richter F. M., Williams C. D., Fedkin A. V. and Wadhwa M. (2014) Evolution of chemical and isotopic compositions of FUN CAIs: Experimental modeling. *Lunar Planet. Sci.* **45**, #2782.

Molini-Velsko C. A. (1983) Isotopic composition of silicon in meteorites. *Ph.D. dissertation*, Univ. Chicago.

Nagahara H. and Ozawa K. (1994) Evaporation of forsterite in H_2 gas. *Geochim. Cosmochim. Acta* **60**, 1445–1459.

Nichols R. H., Wasserburg G. J., and Grimley R. T. (1995) Evaporation of forsterite: identification of gas-phase species via Knudsen cell mass spectrometry. *Lunar Planet. Sci.* **26**, 1047–1048.

Osborn E. F. and Gee K. H. (1969) Phase equilibria at liquidus temperatures for a part of the system CaO-MgO-Al_2O_3-TiO_2-SiO_2 and their bearing on the effect of titania on the properties of blast furnace slag. *Bull. Earth and Mineral Sciences. Experiment Station. No. 85*, 57–80.

Osborn E. F., Roeder P. L., and Ulmer G. C. (1969) Phase equilibria at solidus temperatures in the quaternary system CaO-MgO-Al_2O_3-SiO_2 and their bearing on optimum composition of blast furnace slag and on slag properties. *Bull. Earth and Mineral Sciences. Experiment Station. No. 85*, 1–22.

Paque J. M., Beckett J. R., Barber D. J. and Stolper E. M. (1994) A new titanium-bearing calcium aluminosilicate phase: I. Meteoritic occurrence and formation in synthetic systems. *Meteoritics.* **29**, 673–682.

Richter F. M., Davis A. M., Ebel D. S., and Hashimoto A. (2002) Elemental and isotopic fractionation of Type B calcium-, aluminum-rich inclusions: experiments, theoretical considerations, and constraints on their thermal evolution. *Geochim. Cosmochim. Acta* **66**, 521–540.

Richter F. M., Mendybaev R. A., and Davis A. M. (2006) Conditions in the protoplanetary disk as seen by the Type B CAIs. *Meteorit. Planet. Sci.* 41, 83–93.

Richter F. M., Janney P. E., Mendybaev R. A., Davis A. M., and Wadhwa M. (2007) Elemental and isotopic fractionation of Type B CAI-like liquids by evaporation. *Geochim. Cosmochim. Acta* **71**, 5544–5564.

Sahijpal S. and Goswami J. N. (1998) Refractory phases in primitive meteorites devoid of ^{26}Al and ^{41}Ca: representative samples of first Solar System solids? *Astrophys. J.* **509**, L137–L140.

Simon S. B., Davis A. M., and Grossman L. (1999) Origin of compact type A refractory inclusions from CV3 carbonaceous chondrites. *Geochim. Cosmochim. Acta* **63**, 1233–1248.

Spicuzza M. J., Day J. M. D., Taylor L. A., Valley J. W. (2007) Oxygen isotope constraints on the origin and differentiation of the Moon. *Earth Planet. Sci. Let*., **253**, 254–265.

Stolper E. (1982) Crystallization sequences of Ca-Al-rich inclusions from Allende: An experimental study. *Geochim. Cosmochim. Acta* **46**, 2159–2180.

Stolper E. and Paque J. M. (1986) Crystallization sequences of Ca-Al-rich inclusions from Allende: the effects of cooling rate and maximum temperature. *Geochim. Cosmochim. Acta* **50**, 1785–1806.

Thrane K., Nagashima K., Krot A. N., Bizzarro M. (2008) Discovery of a new FUN CAI from a CV carbonaceous chondrite: Evidence for multistage thermal processing in the protoplanetary disk. *Astrophys. J.*, **680**, L141–L144.

Valley J.W., Kitchen N., Kohn M. J., Niendorf C. R., Spicuzza M. J. (1995) UWG-2, a garnet standard for oxygen isotope ratios: Strategies for high precision and accuracy with laser heating. *Geochim. Cosmochim. Acta* **59**, 5223–5231.

Wang J., Davis A. M., Clayton R. N., Mayeda T. K., and Hashimoto A. (2001) Chemical and isotopic fractionation during the evaporation of the FeO-MgO-SiO_2-CaO-Al_2O_3-TiO_2-REE melt system. *Geochim. Cosmochim. Acta* **65**, 479–494.

Wasserburg G. J., Lee T and Papanastassiou D. A. (1977) Correlated O and Mg isotopic anomalies in Allende inclusions: II. Magnesium. *Geophys. Res. Lett*., **4**, 299–302.

Williams C. D., Wadhwa M., Janney P. E., Hines R. R., Bullock E. S. and MacPherson G. J. (2012) Ti, Si and Mg isotopic systematic of FUN CAI CMS-1. *Meteorit. Planet. Sci.* **47**, *#5102*.

Williams C. D., Ushikubo T., MacPherson G. J., Bullock E. S., Kita N. T., and Wadhwa M (2013) Oxygen isotope systematic of Allende FUN CAI CMS-1. *Lunar Planet Sci.* **44**, #2435.

Williams C. D., Ushikubo T., Bullock E. S., Janney P. E., Hines R. R., Kita N. T., Hervig R. L., MacPherson G. J., Mendybaev R. A., Richter F. M., and Wadhwa M. (2016) Thermal and chemical evolution in the early Solar System as recorded by FUN CAIs: Part I - Petrology, mineral chemistry, and isotopic composition of CMS-1. *Geochim. Cosmochim. Acta* (submitted).

Yamada M., Tachibana S., Nagahara H., and Ozawa K. (2006). Anizotropy of Mg isotopic fractionation during evaporation and Mg self diffusion of forsterite in vacuum. *Planet. Space Sci.,* 5**4**, 1096–1106.

Table 1. Measured chemical bulk composition and magnesium, silicon and oxygen isotopic compositions of starting materials and FUNC evaporation residues.

sample	run duration, min	initial weight, g	final weight, g	weight loss, %	MgO wt%	±2σ	Al_2O_3 wt%	±2σ	SiO_2 wt%	±2σ	CaO wt%	±2σ	SiO_2/Al_2O_3	MgO/Al_2O_3	$\delta^{26}Mg$ ‰	±2σ	$\delta^{25}Mg$ ‰	±2σ	$\delta^{30}Si$ ‰	±2σ	$\delta^{29}Si$ ‰	±2σ	$\delta^{18}O$ ‰	±2σ
B133R-10					11.48	0.09	19.39	0.11	46.00	0.13	23.12	0.11			0.0	0.3	0.0	0.2	0.0	0.3	0.0	0.1		
FUNC starting				0.0	37.9		11.6		42.9		7.6		3.70	3.27										
FUNC-5	0	0.0285	0.0272	4.7	34.09	0.10	13.93	0.08	42.93	0.05	9.05	0.05	3.08	2.45	0.9	0.6	0.5	0.3	-1.4	0.2	-0.6	0.1	12.7	0.1
FUNC-10	5	0.0250	0.0208	16.6	33.53	0.10	15.20	0.12	40.74	0.11	10.48	0.06	2.68	2.21	3.2	0.7	1.6	0.4	1.6	0.1	0.8	0.1	16.2	0.1
FUNC-1	15	0.0334	0.0239	28.6	32.12	0.24	18.16	0.16	37.16	0.11	12.52	0.14	2.05	1.77	10.2	0.6	5.2	0.3	6.0	0.2	3.0	0.1		
FUNC-9	20	0.0276	0.0167	39.7	29.92	0.34	19.78	0.19	35.54	0.11	14.77	0.22	1.80	1.51	16.6	0.5	8.5	0.3	10.4	0.2	5.3	0.1	23.6	0.1
FUNC-3	30	0.0294	0.0158	46.3	27.36	0.34	21.69	0.13	34.24	0.11	16.72	0.26	1.58	1.26	23.9	0.5	12.2	0.3	14.0	0.2	7.1	0.1		
FUNC-7	35	0.0342	0.0155	54.7	23.87	0.07	25.30	0.34	31.63	0.20	19.22	0.24	1.25	0.94	32.8	0.4	16.8	0.2	18.5	0.2	9.4	0.1	30.8	0.1
FUNC-8	40	0.0361	0.0139	61.7	19.08	0.09	31.35	0.24	28.21	0.21	21.37	0.16	0.90	0.61	46.5	0.4	23.9	0.2	22.8	0.1	11.7	0.1		
FUNC-4	45	0.0340	0.0123	63.9	16.51	0.29	32.15	0.54	27.32	0.35	24.03	0.47	0.85	0.51	50.4	0.5	25.9	0.2	25.4	0.2	12.9	0.1	36.8	0.1
FUNC-6	55	0.0390	0.0120	69.3	10.95	0.05	40.16	0.06	22.16	0.07	26.75	0.08	0.55	0.27	69.0	0.6	35.4	0.3	31.5	0.2	16.0	0.1	41.8	0.1

Run duration is time during which the sample was evaporating at 1900ºC.

The isotopic compositions are expressed in the delta notation defined for magnesium, for example, as

$$\delta^{x}Mg = 1000 \times \left[\frac{(^{x}Mg/^{24}Mg)_{sample}}{(^{x}Mg/^{24}Mg)_{standard}} - 1 \right]$$

Table 2. Fractions of magnesium, silicon and oxygen remaining in the FUNC evaporation residues and their isotopic compositions normalized to the zero-time residue.

sample	run duration, min	f_{24Mg}	$\delta^{26}Mg_{t=0}$ ‰	±2σ	$\delta^{25}Mg_{t=0}$ ‰	±2σ	f_{28Si}	$\delta^{30}Si_{t=0}$ ‰	±2σ	$\delta^{29}Si_{t=0}$ ‰	±2σ	f_{16O}	$\delta^{18}O_{t=0}$ ‰	±2σ	$\delta^{17}O_{t=0}$ ‰	±2σ
FUNC-5	0	1.000	0.0	0.6	0.0	0.3	1.000	0.0	0.2	0.0	0.1	1.000	0.0	0.1	0.1	0.1
FUNC-10	5	0.918	2.3	0.7	1.2	0.4	0.889	3.0	0.1	1.4	0.1	0.880	3.5	0.1	1.9	0.1
FUNC-1	15	0.726	9.3	0.6	4.8	0.3	0.669	7.4	0.2	3.7	0.1	0.676				
FUNC-9	20	0.626	15.7	0.5	8.1	0.3	0.592	11.8	0.2	5.9	0.1	0.578	10.9	0.1	5.6	0.1
FUNC-3	30	0.521	23.0	0.5	11.8	0.3	0.518	15.4	0.2	7.7	0.1	0.493				
FUNC-7	35	0.387	31.9	0.4	16.4	0.2	0.410	19.9	0.2	10.0	0.1	0.383	18.1	0.1	9.2	0.1
FUNC-8	40	0.250	45.5	0.4	23.4	0.2	0.296	24.2	0.1	12.3	0.1	0.276				
FUNC-4	45	0.211	49.5	0.5	25.5	0.2	0.279	26.8	0.2	13.5	0.1	0.244	24.2	0.1	12.3	0.1
FUNC-6	55	0.112	68.1	0.6	35.0	0.3	0.181	32.9	0.2	16.6	0.1	0.155	29.1	0.1	14.8	0.1

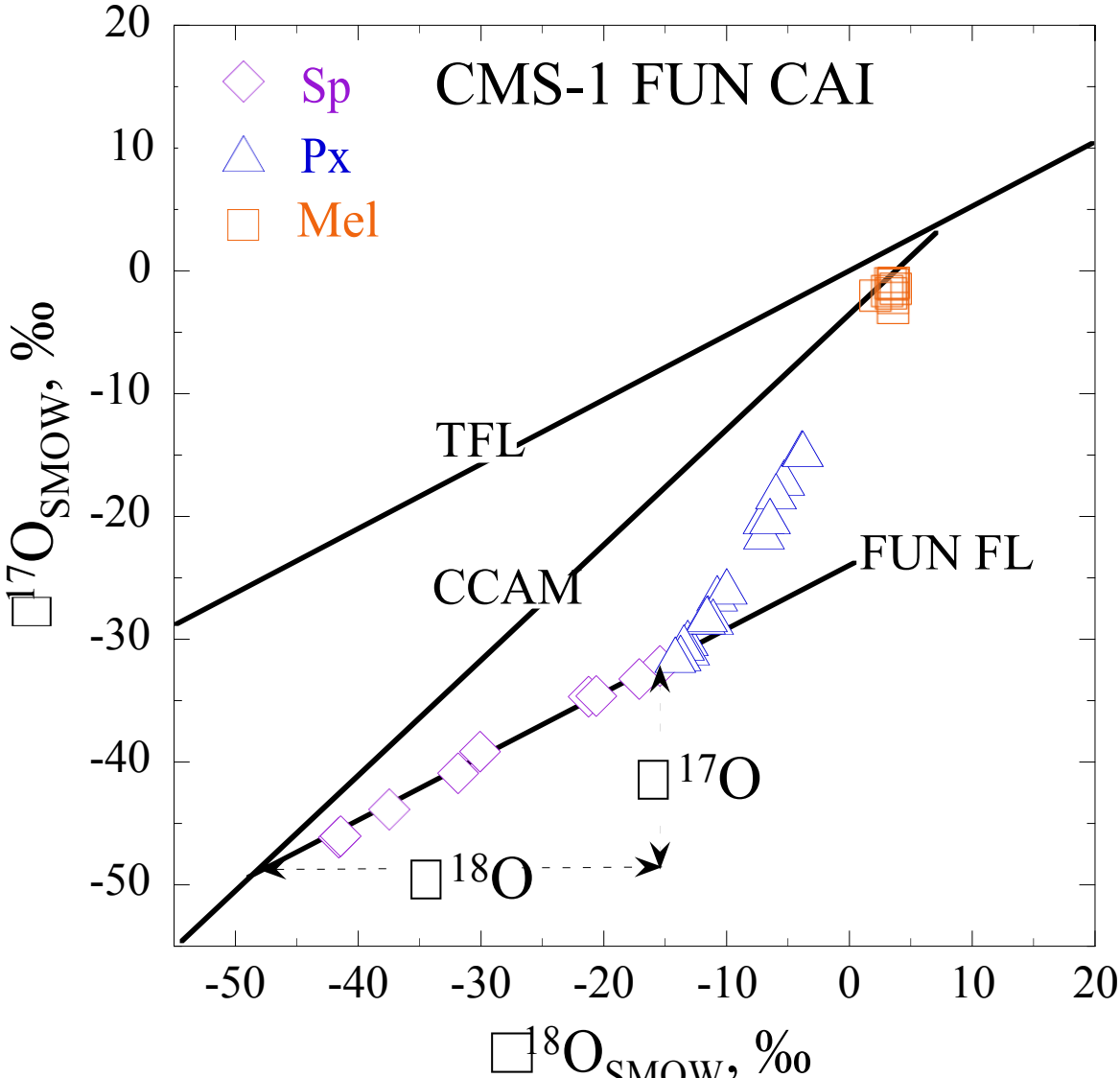
CMS-1 FUN CAI
Sp
Px
Mel
TFL
CCAM
FUN FL
□17O
□18O
□17OSMOW, ‰
□18OSMOW, ‰
20
10
0
-10
-20
-30
-40
-50
-50
-40
-30
-20
-10
0
10
20

Fig. 1

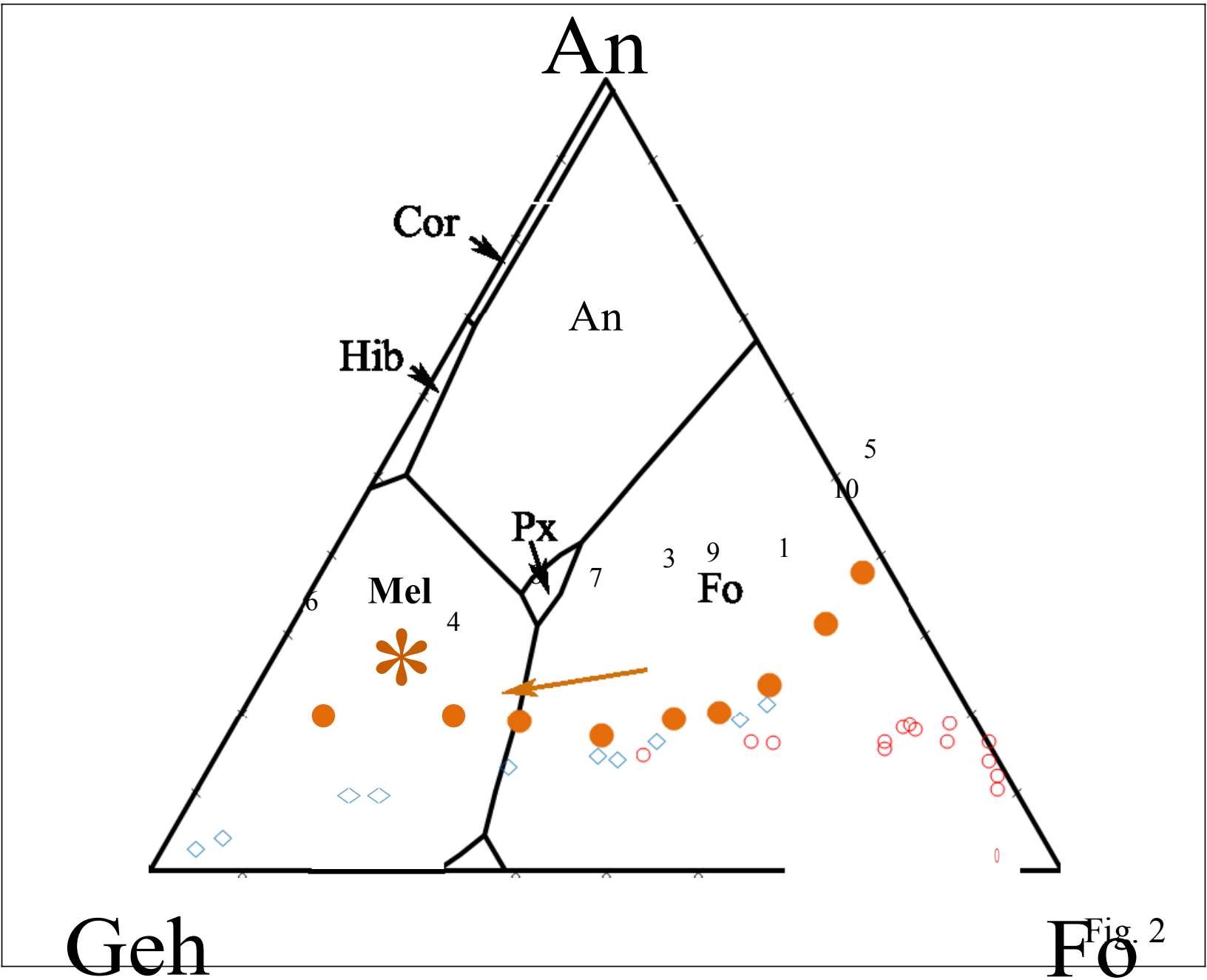

Fig. 2

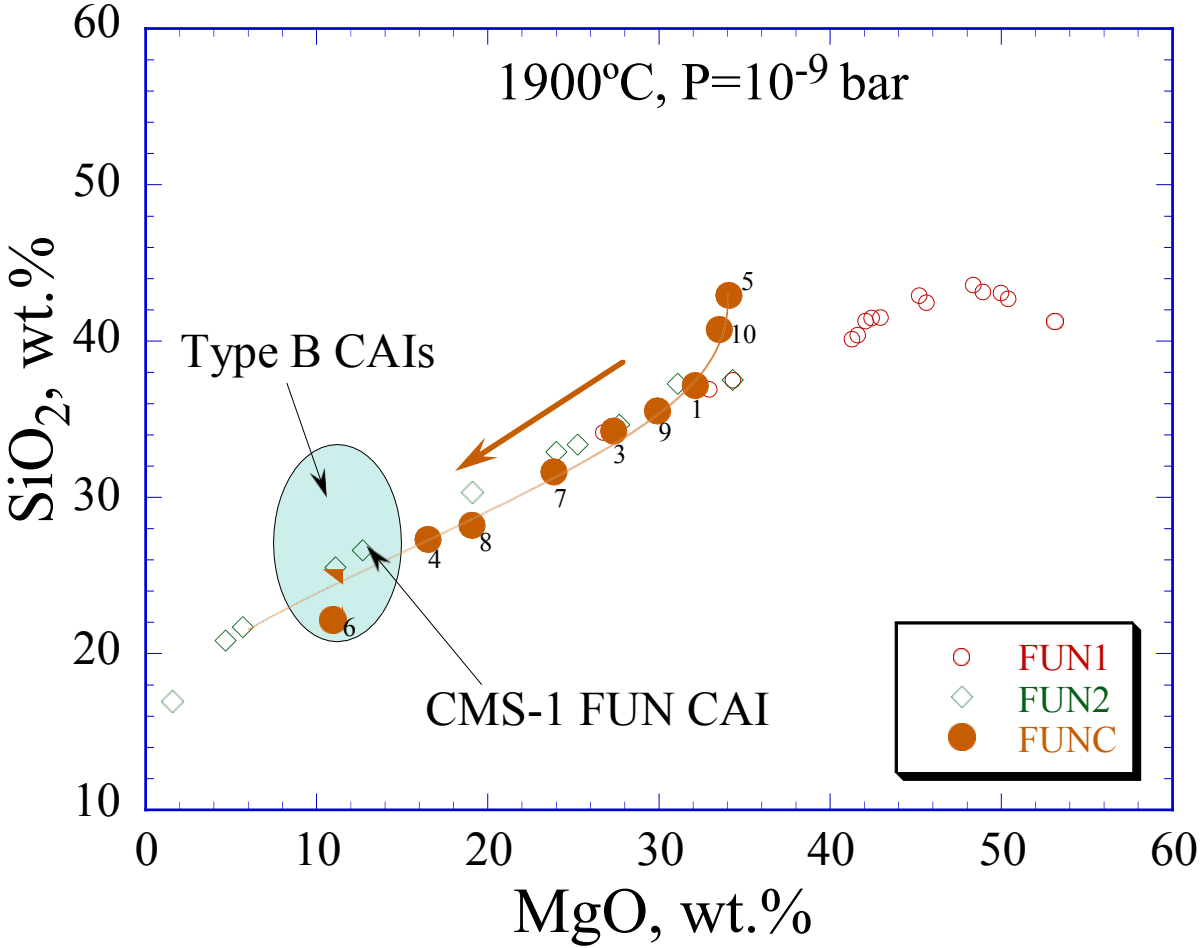
1900°C, P=10-9 bar
Type B CAIs
CMS-1 FUN CAI
FUN1
FUN2
FUNC
SiO2, wt.%
MgO, wt.%
0
10
20
30
40
50
60
1
3
4
5
6
7
8
9
10

Fig. 3

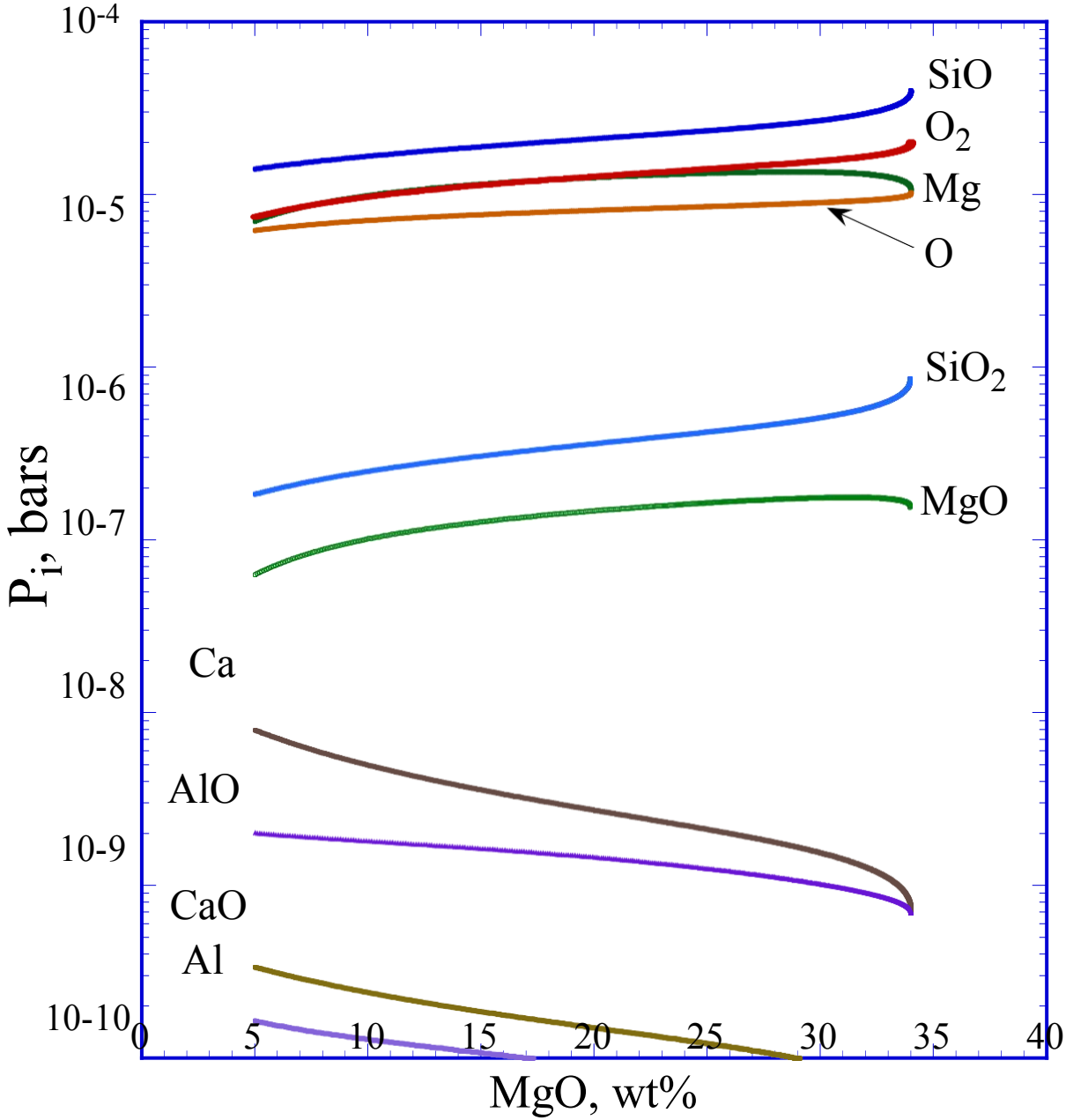
10-4
10-5
10-6
10-7
10-8
10-9
10-10
P_i, bars
0
5
10
15
20
25
30
35
40
MgO, wt%
SiO
O2
Mg
O
SiO2
MgO
Ca
AlO
CaO
Al

Fig. 4

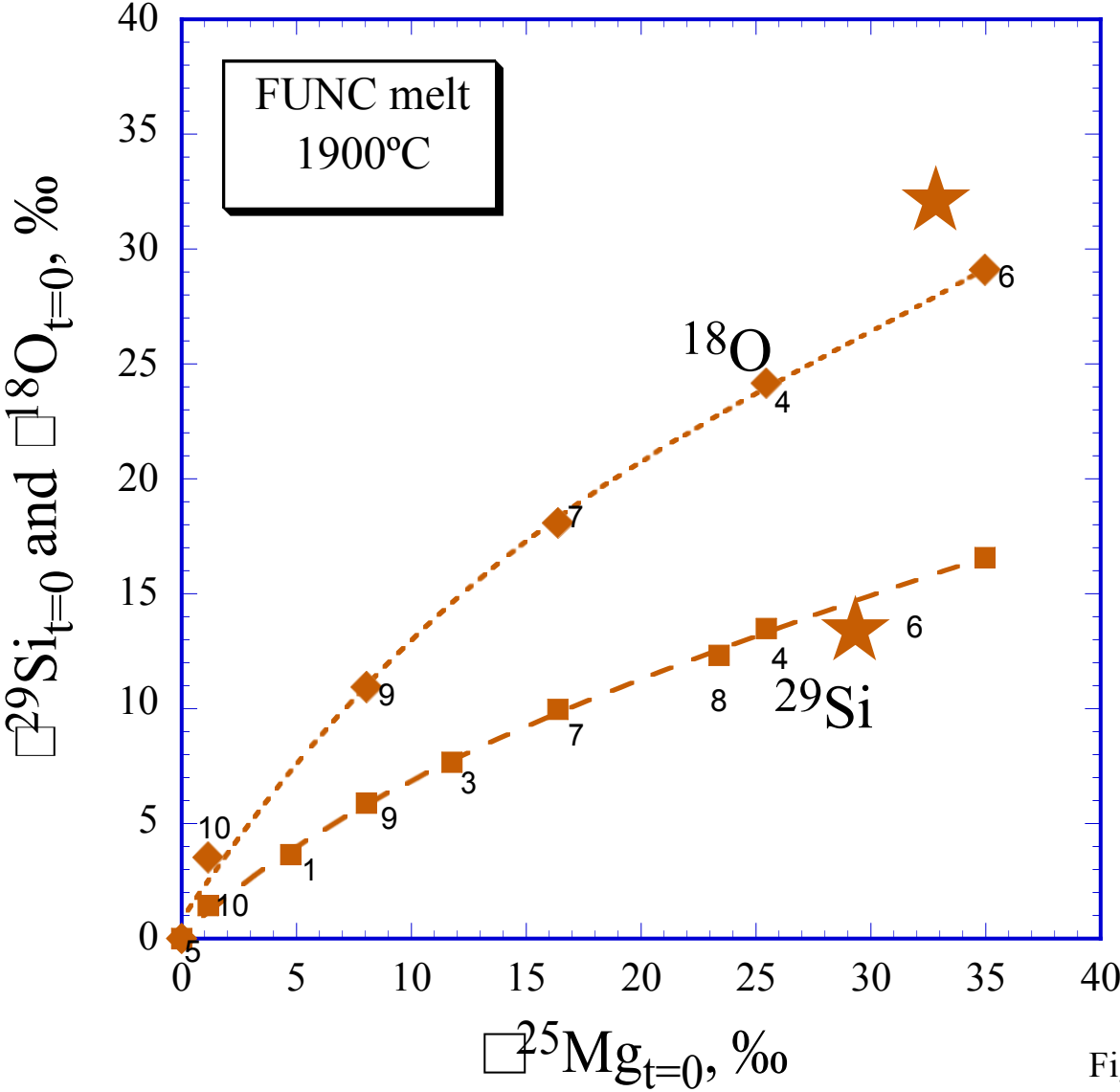
FUNC melt
1900ºC
^{18}O
^{29}Si
$\square^{29}Si_{t=0}$ and $\square^{18}O_{t=0}$, ‰
$\square^{25}Mg_{t=0}$, ‰
0
5
10
15
20
25
30
35
40
10
1
3
9
7
8
4
6
5
10
9
7
4
6

Fig. 5

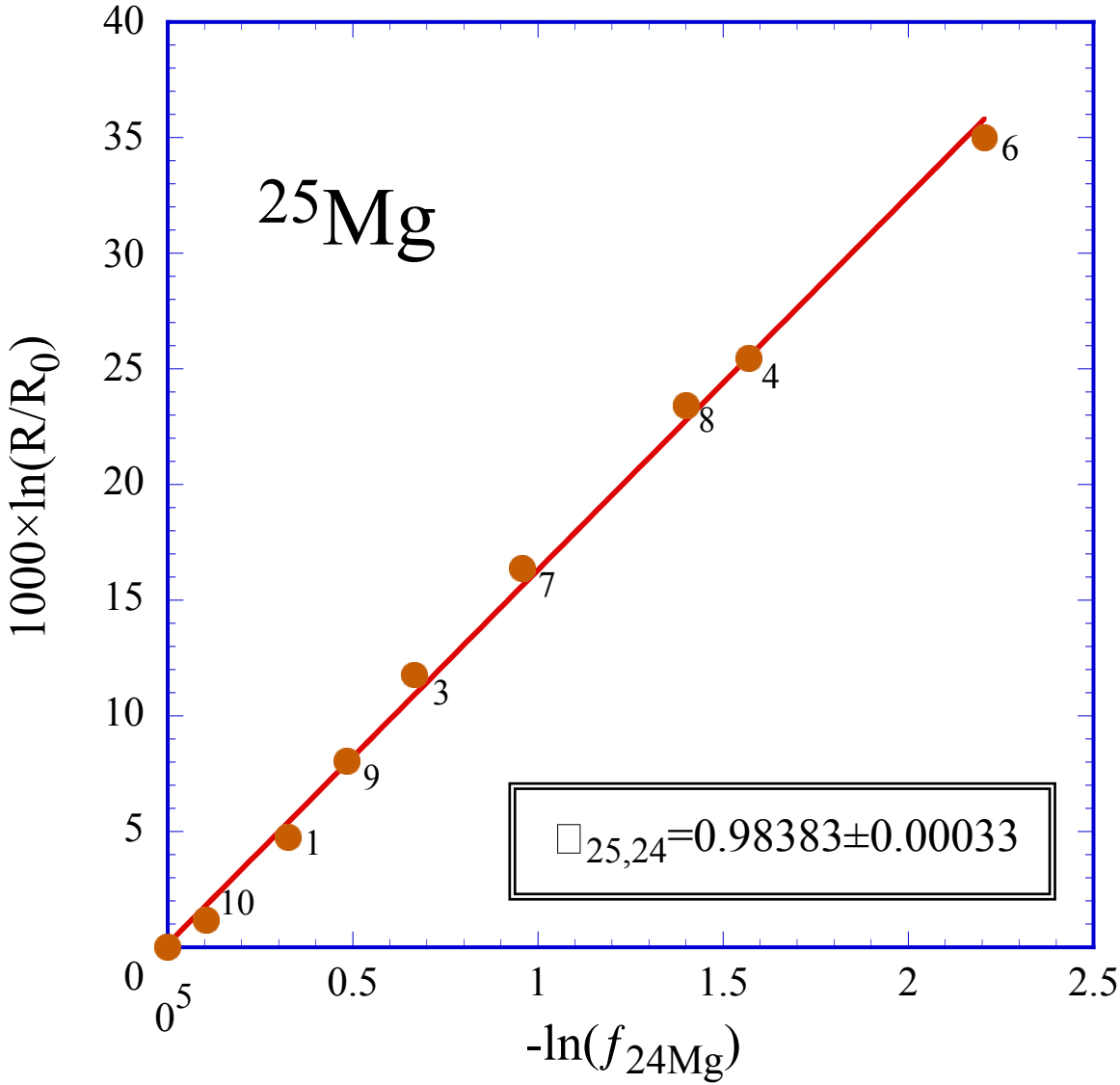
^{25}Mg
□$_{25,24}$=0.98383±0.00033
1000×ln(R/R$_0$)
-ln(f_{24Mg})
0
5
10
15
20
25
30
35
40
0.5
1
1.5
2
2.5
1
3
4
5
6
7
8
9
10

Fig. 6

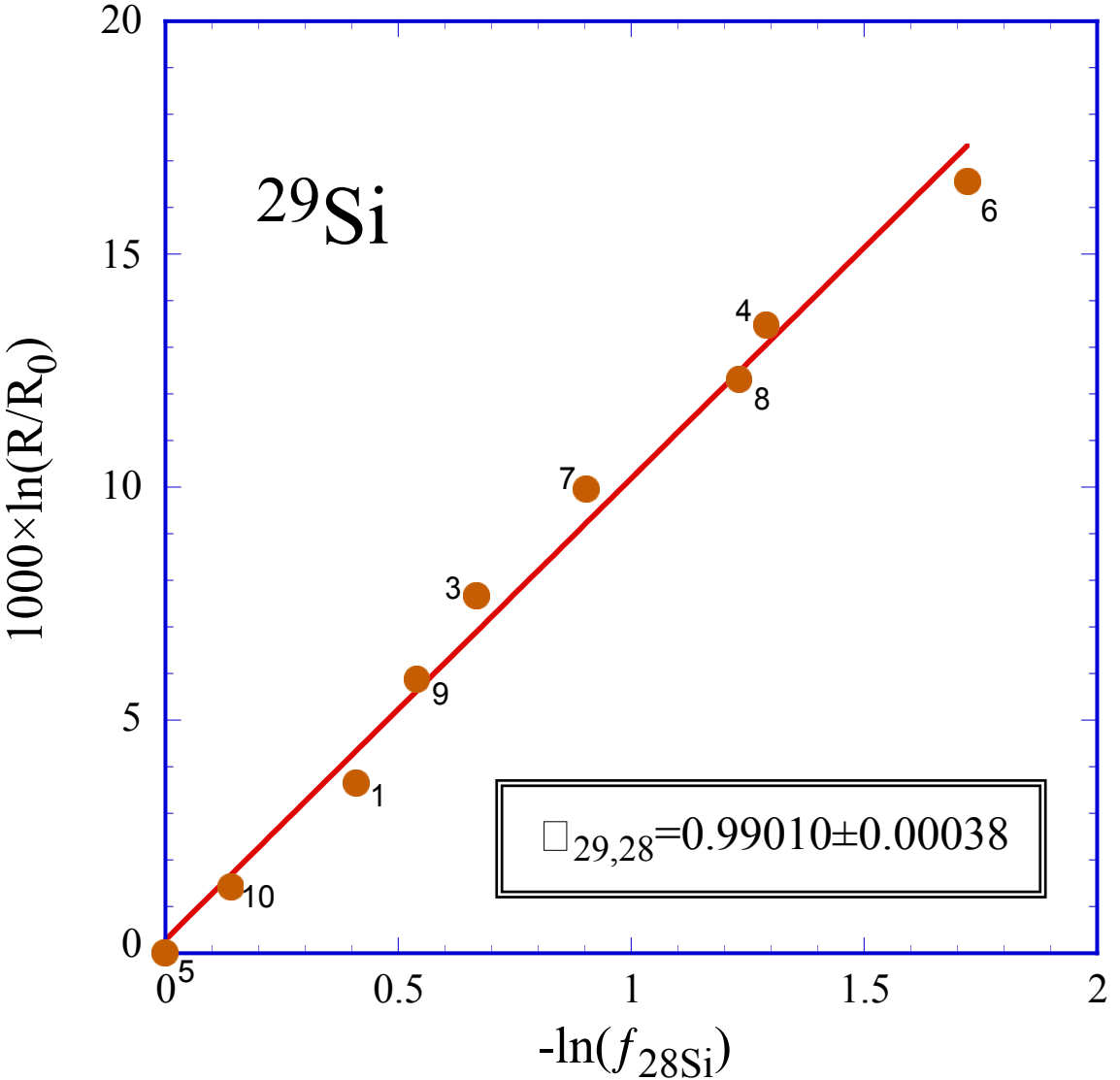
^{29}Si
1000×ln(R/R$_0$)
-ln(f_{28Si})
$\alpha_{29,28}$=0.99010±0.00038
0
5
10
15
20
0.5
1
1.5
2
1
3
4
5
6
7
8
9
10

Fig. 7

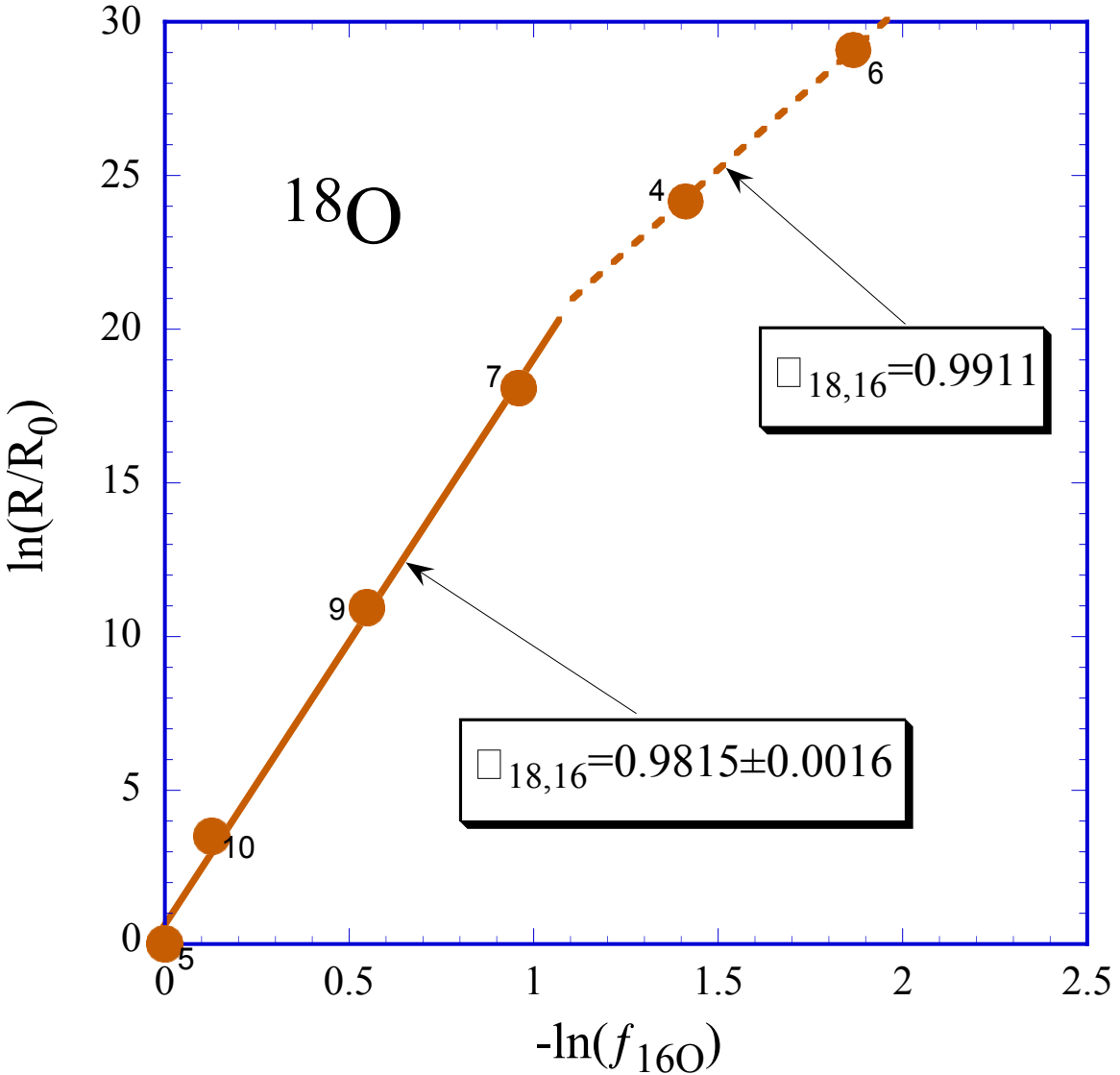
30
25
20
15
10
5
0
0
0.5
1
1.5
2
2.5
ln(R/R0)
-ln(f16O)
18O
6
4
7
9
10
5
□18,16=0.9911
□18,16=0.9815±0.0016

Fig. 8

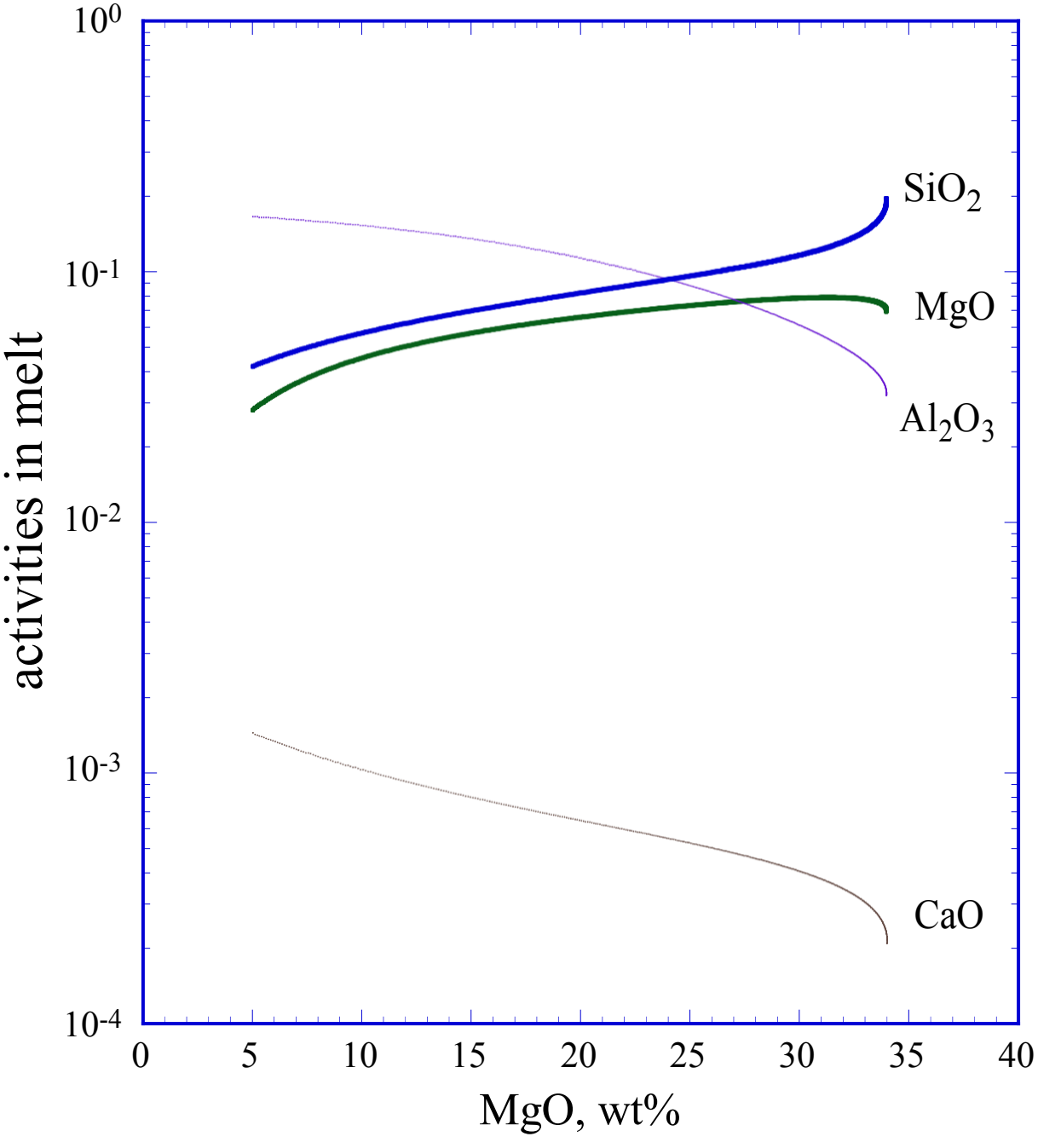
10^0
10^{-1}
10^{-2}
10^{-3}
10^{-4}
activities in melt
0
5
10
15
20
25
30
35
40
MgO, wt%
SiO_2
MgO
Al_2O_3
CaO

Fig. 9

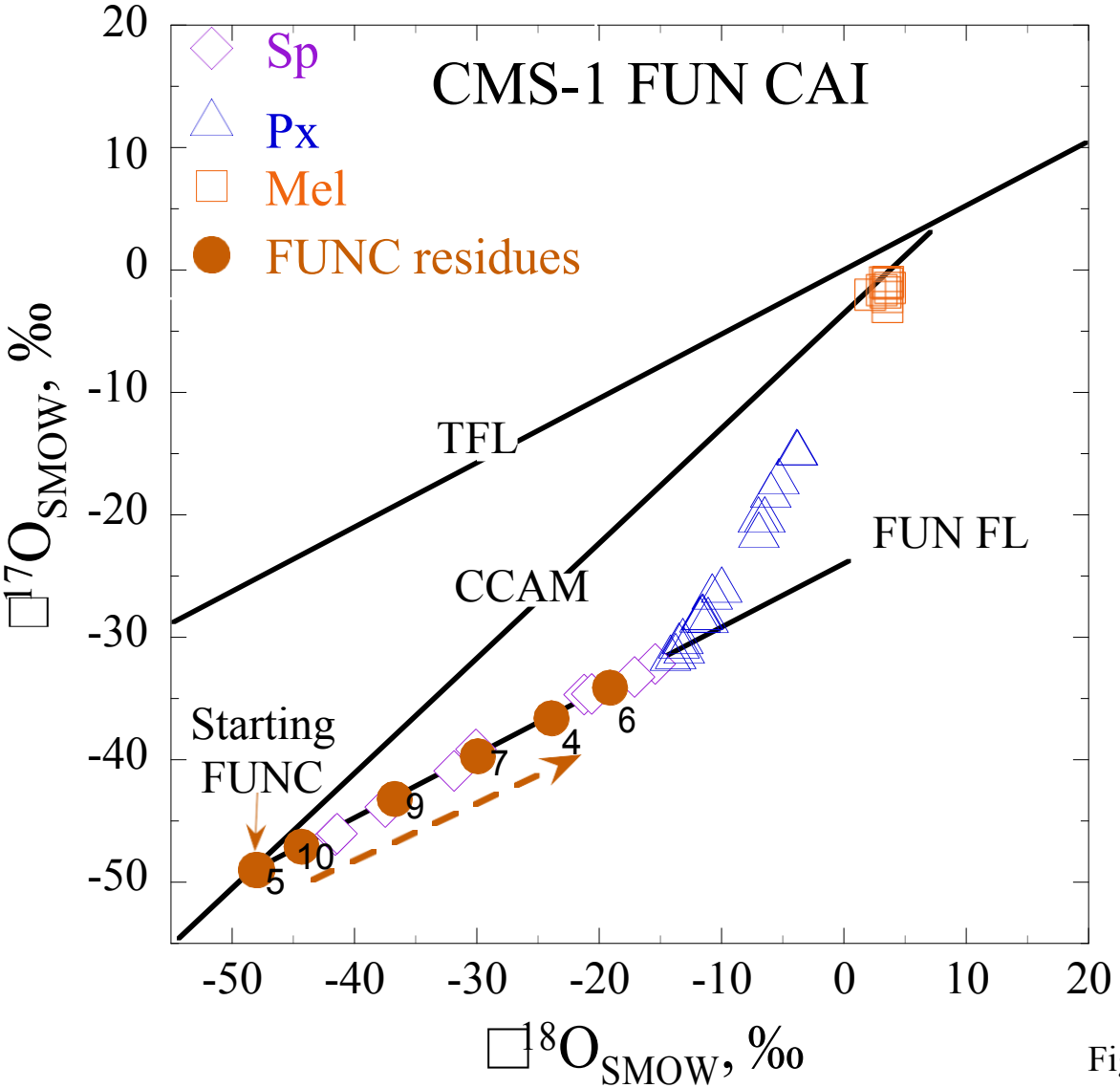
CMS-1 FUN CAI
Sp
Px
Mel
FUNC residues
TFL
CCAM
FUN FL
Starting FUNC
5
10
9
7
4
6
20
10
0
-10
-20
-30
-40
-50
-50
-40
-30
-20
-10
0
10
20
□17OSMOW, ‰
□18OSMOW, ‰

Fig. 10

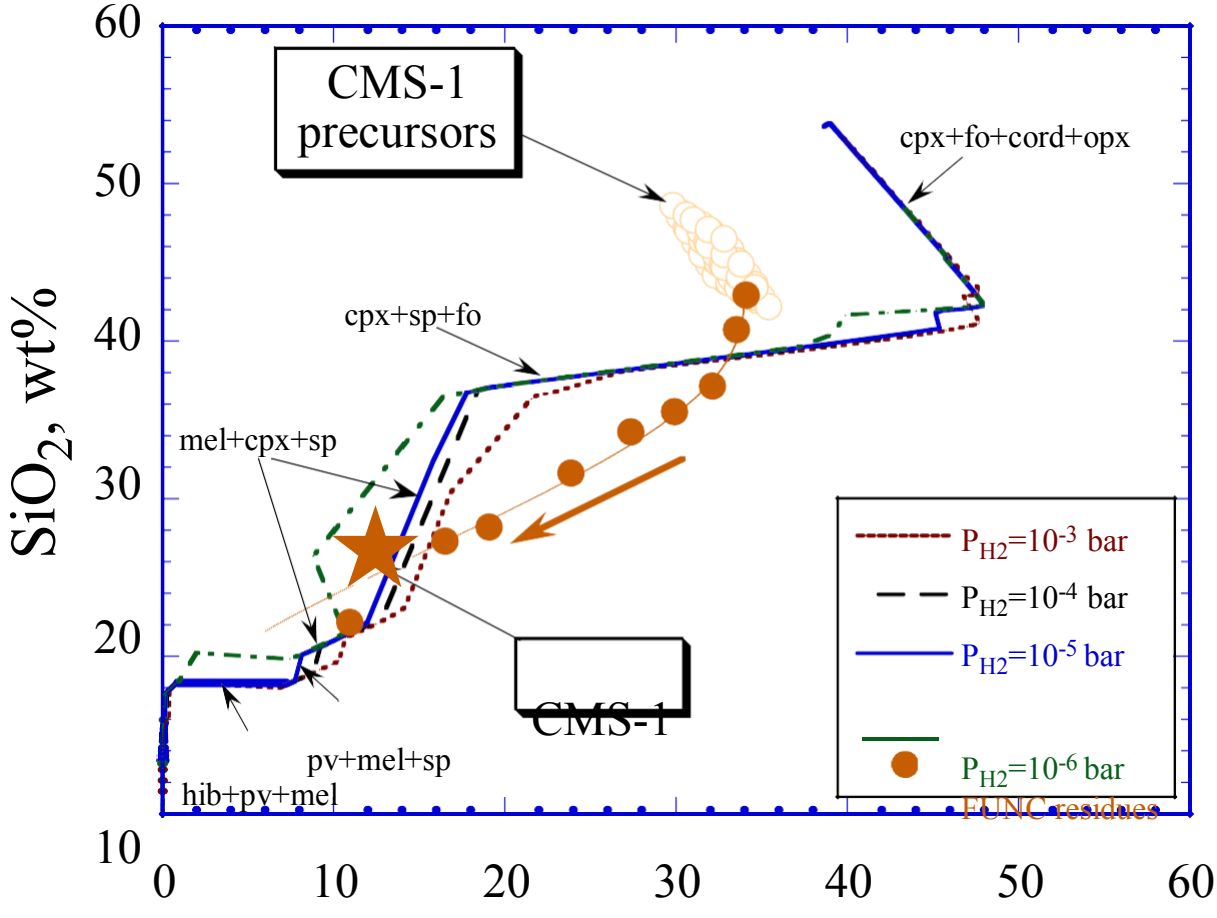
CMS-1
precursors
cpx+fo+cord+opx
cpx+sp+fo
mel+cpx+sp
CMS-1
pv+mel+sp
hib+pv+mel
$P_{H2}=10^{-3}$ bar
$P_{H2}=10^{-4}$ bar
$P_{H2}=10^{-5}$ bar
$P_{H2}=10^{-6}$ bar
FUNC residues
SiO_2, wt%
0
10
20
30
40
50
60

O, wt%

Fig. 11

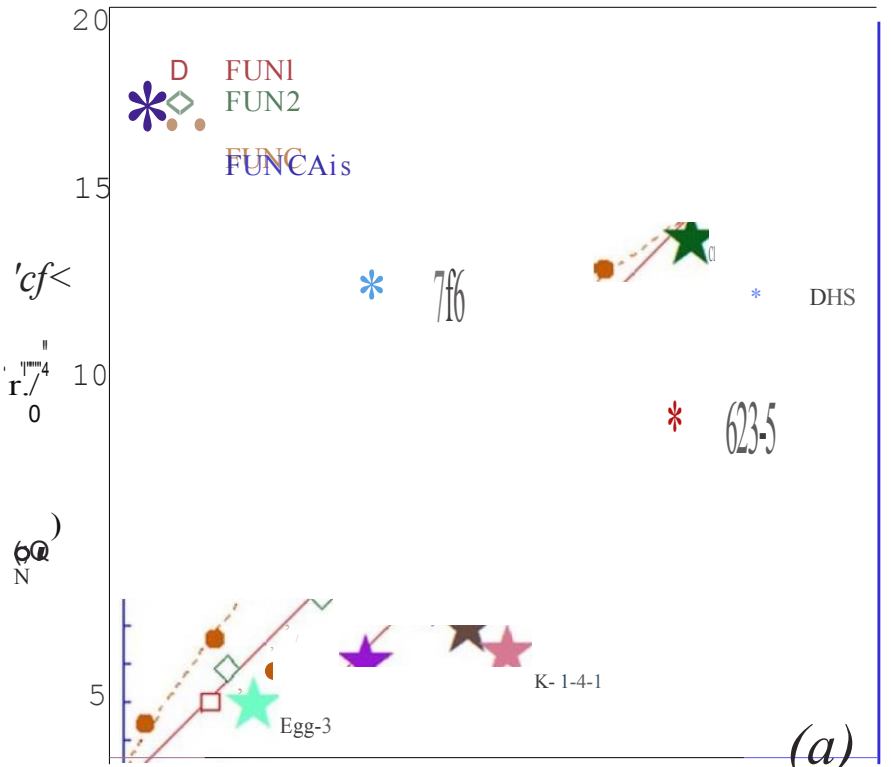
20
15
10
5
D FUNl
FUN2
FUNC
FUNCAis
7f6
DHS
623-5
K- 1-4-1
Egg-3
(a)

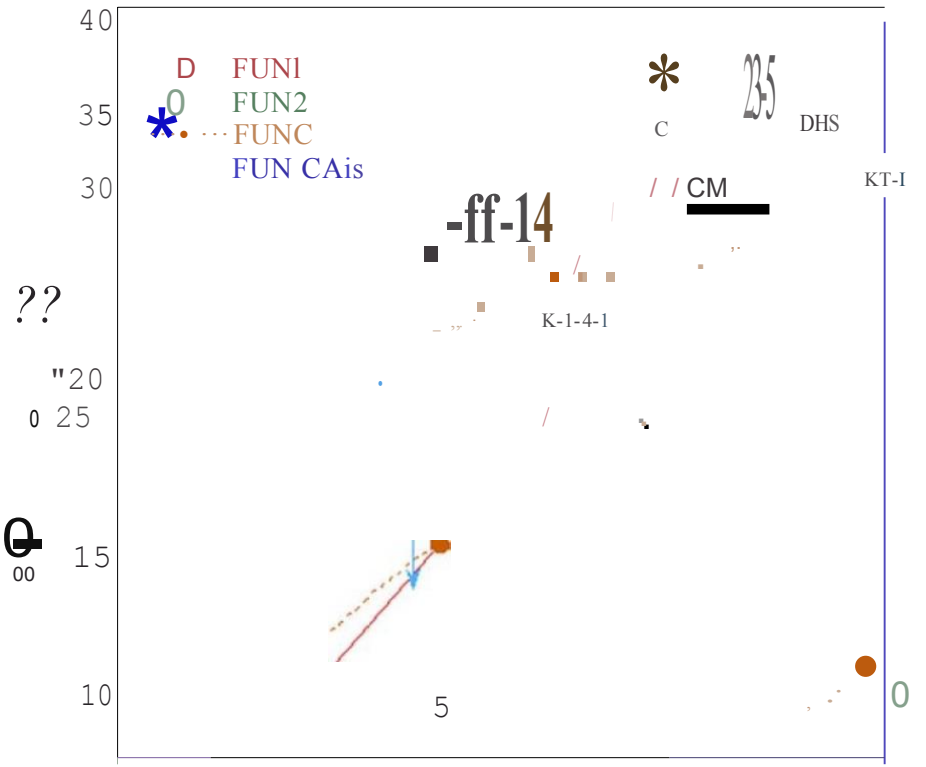
40
35
30
25
20
15
10
5
D FUNl
FUN2
FUNC
FUN CAis
23-5
DHS
C
CM
KT-I
-ff-14
K-1-4-1
0

(b) Fig. 12

Figure 1. Oxygen isotopic composition of individual minerals in Allende FUN CAI CMS-1 (Williams et al., 2016). The degree of mass-dependent oxygen isotopic fractionation due to evaporation (shown as dashed lines) was estimated from the difference between the $\delta^{18}O$ and $\delta^{17}O$ of the most fractionated spinel grain ($\delta^{18}O$= –15.4‰ and $\delta^{17}O$= –32.2‰, Williams et al., 2016) along the FUN FL and the $\delta^{18}O$ and $\delta^{17}O$ values at the intersection of the FUN FL and CCAM lines ($\delta^{18}O$~ –48‰ and $\delta^{17}O$~ –49‰). We use the values of $\Delta^{18}O$~32‰ as our best estimates of oxygen isotopic fractionation caused by evaporation.

Figure 2. Chemical composition of the residues produced by vacuum (~10^{-9} bar) evaporation of the FUNC starting material at 1900ºC plotted in an Anorthite (An) – Gehlenite (Geh) – Forsterite (Fo) ternary diagram projected from spinel. The arrow shows direction in which chemical composition evolves as evaporation proceeds. Composition of most FUNC residues (large filled circles) falls in forsterite stability field, but two the most evaporated residues (FUNC-4 and FUNC-6, see Table 1) have chemical composition within the melilite stability field. The bulk chemical composition of FUN CAI CMS-1 is shown as a star. Also shown are the chemical compositions of the evaporation residues from the FUN1 (open circles) and FUN2 (open diamonds) experiments (Mendybaev et al., 2013a). Note that the location of a point in this diagram is very sensitive to concentrations of MgO and SiO_2 such that adding 1.5 wt% MgO and subtracting 1.5 wt% SiO_2 to the reported bulk composition of CMS-1 CAI (Williams et al., 2016) will bring its position down to the trend established by the experimental FUNC residues. The stability fields of melilite (Mel), forsterite (Fo), anorthite (An), pyroxene (Px), cordierite (Cor), and hibonite (Hib) are shown. Numbers next to the

closed circles are sample numbers from FUNC evaporation experiments (e.g., 6 means sample FUNC-6).

Figure 3. Chemical composition of the FUNC residues in MgO – SiO_2 composition space. Also shown is the compositional trajectory of the FUNC residues calculated the same way as described by Grossman et al. (2000) and assuming that $\gamma_{SiO}/\gamma_{Mg} = 2.1$, where γ_{SiO} and γ_{Mg} are the evaporation coefficients of $SiO_{(g)}$ and $Mg_{(g)}$ in the Hertz-Knudsen equation (see text for details). The typical range of compositions of Type B CAI is shown as a reference. Numbers next to the closed circles are sample numbers (e.g., 6 means sample FUNC-6).

Figure 4. The equilibrium vapor pressures of major gaseous species over the evaporating FUNC melt at 1900ºC calculated assuming that $\gamma_{SiO}/\gamma_{Mg} = 2.1$ to fit the FUNC experimental evaporation trajectory in Fig. 3. Degree of the evaporation is expressed as MgO content of the residual FUNC melt (Fig. 3). $SiO_{(g)}$ and $Mg_{(g)}$ are the major silicon- and magnesium-bearing species over the evaporating FUNC melt while the partial pressures of $SiO_{2(g)}$ and $MgO_{(g)}$, the next most abundant silicon- and magnesium-bearing species, are lower by a factor of >50. The most abundant oxygen-bearing species is $SiO_{(g)}$ while $O_{2(g)}$ and $O_{(g)}$ are less abundant by factor of ~2 to 4. As silicon and magnesium evaporate, the residual FUNC melt becomes enriched in the refractory calcium and aluminum resulting in decrease of partial pressures of silicon- and magnesium bearing species and increase of that of calcium- and aluminum-bearing species.

Figure 5. Magnesium, silicon and oxygen isotopic compositions of the FUNC evaporation residues relative to the sample FUNC-5 (δ^{29}Si≡0, δ^{25}Mg≡0, δ^{18}O≡0) that was produced in the zero-time evaporation experiment (the data are from Table 2). Long dashed curve shows relationship between δ^{29}Si and δ^{25}Mg, and the short dashed curve shows relationship between δ^{18}O and δ^{25}Mg. Also shown by the star symbol is the isotopic compositions of CMS-1 (δ^{25}Mg = 32.72±0.50 and δ^{29}Si= 15.54±0.27 are the measured values relative to DSM-3 and NBS-28 respectively as reported by Williams et al., 2016; the quantity Δ^{18}O =32‰ is our estimate of oxygen isotopic fractionation caused by evaporation of CMS-1 precursor, see Fig. 1 and text for details). The analytical uncertainties are less than the symbol size. Numbers next to the symbols are sample numbers (e.g., 6 means sample FUNC-6).

Figure 6. Rayleigh plot of the magnesium isotopic fractionation of the FUNC evaporation residues as a function of the amount of ^{24}Mg remaining in the residue. When plotted in this way the slope of the best fitting line through the data of a set of evaporation residues from a common initial composition is a measure of $1 - \alpha_{25,24}$, where $\alpha_{25,24}$ is the kinetic magnesium isotope fractionation factor. The FUNC data result in an estimate of $\alpha_{25,24}$ = 0.98383±0.00033, which is the same as 0.98372±0.00041 obtained for FUN 1 and FUN 2 melts (Mendybaev et al., 2013).The analytical uncertainties are less than the symbol size. Numbers next to the symbols are sample numbers (e.g., 6 means sample FUNC-6).

Figure 7. Rayleigh plot of the silicon isotopic fractionation of the FUNC evaporation residues as a function of the amount of ^{28}Si remaining in the residue. The silicon isotopic composition of all FUNC residues results in $\alpha_{29,28}$ = 0.99010±0.00038 which is the

same as 0.9899±0.0004 obtained for FUN 1 and FUN 2 melts (Mendybaev et al., 2013). The analytical uncertainties are less than the symbol size. Numbers next to the symbols are sample numbers (e.g., 6 means sample FUNC-6).

Figure 8. Rayleigh plot of the oxygen isotopic fractionation of the FUNC evaporation residues as a function of the amount of ^{16}O remaining in the residue. The oxygen isotopic composition of FUNC residues with chemical composition in the forsterite stability field (see Fig. 2) plot along a line fit by $\alpha_{18,16}$ = 0.9815±0.0016 which is the close to 0.9786±0.0015 obtained for FUN 1 and FUN 2 melts (Mendybaev et al., 2013). The two most evaporated residues (FUNC-4 and FUNC-6) with composition in the melilite stability field (see Fig. 2) are fit by $\alpha_{18,16}$ ~ 0.9911 (dashed line) which is the close to 0.9886 obtained for FUN 2 melts with composition in the melilite stability field (Mendybaev et al., 2013). The analytical uncertainties are less than the symbol size. Numbers next to the symbols are sample numbers (e.g., 6 means sample FUNC-6).

Figure 9. Activities of MgO, SiO_2, Al_2O_3 and CaO in the evaporating FUNC melt calculated using γ_{SiO}/γ_{Mg} = 2.1 as in Figs. 3 and 4. The degree of evaporation is expressed as the MgO content in the residual melt. Note the initial rapid decrease of a_{SiO2} due to faster evaporation of silicon compared to magnesium, which increases a_{MgO}. After this initial stage the activities of MgO and SiO_2 become essentially parallel to each other resulting in a constant relative evaporation rates of magnesium and silicon as evaporation proceeds (see text for details).

Figure 10. Oxygen isotopic composition of individual minerals in FUN CAI CMS-1 (open symbols; Williams et al., 2016) and FUNC evaporation residues (closed circles). Here

we assumed that the oxygen isotopic composition of the starting FUNC melt (sample FUNC-5) was $\delta^{17}O$= –49‰ and $\delta^{18}O$= –48‰ (the values at the intersection of CCAM and FUN fractionation lines). Oxygen isotopic composition of the evaporation residues relative to starting FUNC-5 material ($\delta^{17}O$= –49‰ and $\delta^{18}O$= –48‰) was calculated using Table 2. The dashed arrow shows the direction in which the oxygen isotopic composition changes as evaporation proceeds. The figure illustrates that the oxygen isotopic composition of the experimental FUNC residues plot along the FUN FL defined by spinel grains of CMS-1. Numbers next to the closed circles are sample numbers (e.g., 6 means sample FUNC-6).

Figure 11. The trajectories in MgO-SiO_2 space of condensates from a cooling solar composition gas calculated for total pressure of $P_{H2}=10^{-3}$, 10^{-4}, 10^{-5} and 10^{-6} bars. The mineral assemblages (hib – hibonite, pv – perovskite, mel – melilite, sp – spinel, cpx – clinopyroxene, fo – forsterite, cord – cordierite, opx – orthopyroxene) predicted to be in equilibrium with the gas along condensation trajectories are shown (see Fig. 4 of Grossman et al., 2008 for details). The filled circles are composition of the FUNC evaporation residues with the arrow showing direction in which the melt evaporated. Shown as a cloud of open circles is composition of CMS-1 precursor calculated using measured enrichments in heavy silicon and magnesium isotopes in CMS-1 to calculate the amount of SiO_2 and MgO lost by evaporation and adding this to the present bulk composition of CMS-1. The cloud of possible CMS-1 precursor compositions takes into account uncertainties in the measured values of $\delta^{29}Si$ and $\delta^{25}Mg$ in CMS-1 as well as uncertainties in the experimentally determined values of $\alpha_{25,24}$ and $\alpha_{29,28}$.

Figure 12. Relationships between δ^{29}Si and δ^{25}Mg (*a*) and δ^{18}O and δ^{25}Mg (*b*) in FUN CAIs (shown as stars). δ^{25}Mg and δ^{29}Si values in panel (*a*) are from Clayton et al. (1988), Brigham (1990) and Davis et al. (1991). The δ^{18}O values in panel (*b*) are our estimates of the oxygen isotopic fractionation caused by evaporation using data of Davis et al. (2000), Krot et al. (2014), and Williams et al. (2016). Also shown are data for the FUNC (solid circles), FUN1 (open squares) and FUN2 (open diamonds) evaporation residues with composition within the forsterite stability field (Fig. 2). The solid lines are best fits to the δ^{29}Si versus δ^{25}Mg data and for the δ^{18}O versus δ^{25}Mg data from FUN1 and FUN2 experiments (Mendybaev et al., 2013a). The dotted lines are the best fits of the FUNC data. The dashed line in (*b*) is an extrapolation of the δ^{18}O-δ^{25}Mg correlation line of the FUN1 and FUN2 data.